

**Title:**

Explaining Patterns of Neural Activity in the Primary Motor Cortex Using Spinal Cord and Limb  
Biomechanics Models

**Authors:**

Ehud Trainin<sup>1</sup>, Ron Meir<sup>1</sup>, Amir Karniel<sup>2</sup>.

1) Department of Electrical Engineering, Technion – Israel Institute of Technology, Haifa 32000, Israel.

2) Department of Biomedical Engineering, Ben-Gurion University of the Negev, Beer-Sheva 84105, Israel.

**Running head:**

Control Theory Predicts Neural Activity in Motor Cortex

**Contact information:**

Ron Meir, Department of Electrical Engineering, Technion, Haifa 32000, Israel. [rmeir@ee.technion.ac.il](mailto:rmeir@ee.technion.ac.il)

Phone: 972-4-829-4658

**Abstract**

What determines the specific pattern of activation of primary motor cortex (M1) neurons in the context of a given motor task? We present a systems level physiological model describing the transformation from the neural activity in M1, through the muscle control signal, into joint torques and down to endpoint forces and movements. The redundancy of the system is resolved by biologically plausible optimization criteria. The model explains neural activity at both the population, and single neuron, levels. Due to the model's relative simplicity and analytic tractability, it provides intuition as to the most salient features of the system, as well as a possible causal explanation of how these determine the overall behavior. Moreover, it explains a large number of recent observations, including the temporal patterns of single-neuron and population firing rates during isometric and movement tasks, narrow tuning curves, non-cosine tuning curves, changes of preferred directions during a task, and changes of preferred directions due to different experimental conditions.

## Introduction

The primate motor system is a highly complex system leading to sophisticated motor activities resulting from the concerted activity of many cortical, sub-cortical and skeletal modules involving multiple feedback loops (Dum and Strick, 2005). One of the key components in this system is the primary motor cortex (M1), which plays a major role in voluntary limb movement. Projections from M1 influence muscles through direct synapses onto motor neurons and indirectly through spinal inter-neurons (Kandel et al., 2001). It is now well understood that M1 is highly heterogeneous (Alexander and Crutcher, 1990; Crutcher and Alexander, 1990; Kakei et al., 1999; Ashe 2005), and that different populations in M1 represent different motor control signals, and therefore cannot be uniformly interpreted. However, physiology provides evidence that some M1 neurons are highly correlated with muscle activity (e.g., Fetz and Cheney, 1982; Morrow and Miller, 2003). We refer to such neurons as *muscle related cells*. Our model is aimed at explaining the functional behavior of these muscle related cells in M1 in the context of arm movement.

Many statistical models (e.g., Georgopoulos et al., 1982; Sanger, 1996; Paninski et al., 2004) describe how neuronal activity of single neurons changes with hand variables, and play an important role in neural prosthetic applications (Schwartz 2004). However, these approaches do not provide answers to the following basic questions. (i) How do neural activities, projected from the motor cortex towards the spinal cord, result in hand movement and force? (ii) Given the redundancy of the controlled system (Bernstein, 1967), how does the brain select specific control signals in order to achieve a motor task? The model provided here directly addresses these questions. In particular, our study is focused on the profound influence of some of the plant's properties on the control signal's behavior, where by plant we refer to the spinal-musculo-skeletal system. Understanding the spinal cord and the limb biomechanics is essential to explaining the motor control signals descending from the brain to the spinal cord. Our systems level physiological model describes the transformation from the neural activity in M1, through the muscle control signal (MCS), into muscle forces, joint torques and down to endpoint forces and movements. The redundancy of the system is resolved by adding biologically plausible optimization criteria.

Our model aims at being the 'simplest' physiological model able to predict the complex patterns of activity of muscle related neurons in M1. Despite its relative simplicity, the model captures key features of the spinal cord and of the biomechanical system in the context of the tasks studied. In particular, limb mechanics, muscle unidirectionality and the finite time response of the muscles and the spinal cord are key properties of the system, responsible for basic features of the observed neural activity. Our model makes specific predictions about novel experimental situations, and is consistent with current experimental results.

## Methods

Our model is aimed at predicting the neural activity of a subset of primary motor cortex neurons, which contribute linearly and additively to the input of the motor-neuron pools (whether such a contribution is achieved through direct or indirect connections to motor-neurons). We refer to such neurons as muscle related neurons, and assume that these cells include the cortico-motor-neurons and, possibly, some of the other neurons in M1. It is expected that many of the non-cortico-motor-neurons in M1 do not possess such a linear and additive contribution to the muscle control signal, as they either project to other parts of the spinal cord, or do not project to the spinal cord at all.

We consider voluntary movement tasks, implying that the control signal is initiated from the motor cortex. Moreover, we consider simple trained tasks, motivating the assumption that the control signal is reproducible to a reasonable degree of accuracy, and that it is optimized for the task. Additionally, we assume well-trained tasks, which do not require the hand to achieve high accuracy or to retain stability against significant perturbations. This implies that the brain does not use significant co-activation of antagonist muscles in order to increase the hand's impedance (Hogan, 1984; Hogan, 1989; Osu et al., 2004).

Two essential properties related to the plant model are the number of degrees of freedoms (DOF) of the joints, and the number of muscles spanning the arm's joints. Arm models of varying complexity have been introduced in the literature, starting from 2-DOF with 2-muscles (e.g., Harris and Wolpert 1998) and up to 13-DOF with 42 muscle bundles (Garner and Pandy, 2001). Our solution is general, in the sense that it assumes neither a specific number of DOF, nor a specific number of muscles. We use general formulae, in which  $D$  stands for the number of DOF and  $M$  stands for the number of muscles. Additionally we illustrate the model and its solution using a relatively simple arm model with 2-DOF ( $D = 2$ ) and 6 muscles ( $M = 6$ ).

The model addresses the following issues:

- 1) The relation between end-point force and joint torques.

- 2) The relation between joint torques and joint movement.
- 3) The relation between equivalent muscle forces and joint torques.
- 4) The relation between MCSs and muscular force.
- 5) Resolving the redundancy of MCSs by an optimality criterion.
- 6) The relation between neuron activities and the MCS.
- 7) Resolving the redundancy of neuron activities by an optimality criterion.

Next, we present a detailed description of the model, and refer the reader to Figure 1a for a graphical explanation.

#### *Hand Position and Joint Angles*

We assume that joint angle trajectories (or some equivalent data) are given by either direct measurements or by some model. The transformation between end point position and joint angles is given by

$$(1) \quad \underline{P} = f(\underline{\theta})$$

where  $\underline{P}$  is a vector designating hand position and  $\underline{\theta}$  is a vector of joint angles. The function  $f$  is nonlinear, and uses the lengths of the arm's links as parameters. It can be calculated based on multiplication of transformation matrices (Asada and Slotine, 2000; Spong et al., 2006).

The kinematic equations of a bi-joint planar arm (see Fig. 2a) are given in Appendix B.

#### *Joints Torques*

Once joint angles and external force trajectories are given, it is possible to calculate the total torque exerted by the muscles at each joint. The joint torque  $\underline{\tau}$  is given by

$$(2) \quad \underline{\tau} = -\underline{\tau}_D - \underline{\tau}_S,$$

where  $\underline{\tau}_S$  is the joint torque due to the external force and  $\underline{\tau}_D$  is the joint torque due to arm movement.

These torques are derived using the following transformations and relations, which are standard in the Robotics literature (e.g., Asada and Slotine, 2000; Spong et al., 2006).

The transformation between end-point force and joint torques (statics) is given by

$$(3) \quad \underline{\tau}_S = \underline{\underline{J}}^T(\underline{\theta}) \underline{F}^{(ex)},$$

where  $\underline{\tau}_S$  is the vector of joint torques,  $\underline{F}^{(ex)}$  is the external force vector and  $\underline{\underline{J}}$  is the manipulator Jacobian.

The manipulator Jacobian  $\underline{\underline{J}}$  is a  $N \times D$  matrix, where  $N$  is the external space dimensionality and  $D$  is the number of DOF. It is derived from Equation (1) according to

$$\underline{\underline{J}} = \begin{bmatrix} \frac{\partial P_1}{\partial \theta_1} & \frac{\partial P_1}{\partial \theta_2} & \cdot & \cdot & \frac{\partial P_1}{\partial \theta_D} \\ \cdot & \cdot & \cdot & \cdot & \cdot \\ \frac{\partial P_N}{\partial \theta_1} & \frac{\partial P_N}{\partial \theta_2} & \cdot & \cdot & \frac{\partial P_N}{\partial \theta_D} \end{bmatrix}$$

The Jacobian of a bi-joint planar arm is given in Appendix B.

The relation between torques and movement (dynamics) is given by

$$(4) \quad \underline{\tau}_D = \underline{\underline{M}}(\underline{\theta}) \frac{d^2 \underline{\theta}}{dt^2} + \underline{\underline{C}}\left(\underline{\theta}, \frac{d\underline{\theta}}{dt}\right) + \underline{\underline{G}}(\underline{\theta}),$$

where  $\underline{\tau}$  is the vector of joint torques,  $\underline{\theta}$  is a vector of joint angles,  $\underline{\underline{M}}$  accounts for inertial forces,  $\underline{\underline{C}}$  accounts for velocity-dependent forces and  $\underline{\underline{G}}$  represents the influence of gravity. The derivation of the dynamical equation for a given arm model can be done using Euler-Lagrange equations (Asada and Slotine, 2000; Spong et al., 2006). The explicit form of (4) for a bi-joint arm without gravity (see Fig. 2a) is given in Appendix B.

### *Musculoskeletal Geometry*

An *equivalent muscle* describes an anatomical muscle, or a synergetic group of anatomical muscles, along with the spinal cord circuits related to these muscles. The moment arm describes the relationship between the equivalent muscle force and the torque produced at each joint. In our model, it is assumed that the moment arm is constant for all joint angles so that  $\tau_{ij}(t) = R_{ij}F_i(t)$ , where  $\tau_{ij}(t)$  is the moment produced by equivalent muscle  $i$  on joint  $j$  and  $R_{ij}$  is the (constant) moment arm of equivalent muscle  $i$  acting on joint  $j$ .

The total joint moment at joint  $j$  is given by  $\tau_j(t) = \sum_{i=1}^M R_{ij}F_i(t)$   $j = 1, 2, \dots, D$ , or

$$(5) \quad \underline{\tau}(t) = \underline{R}^T \underline{F}(t),$$

where  $\underline{R}$  is the  $M \times D$  matrix composed of the arm moments  $R_{ij}$ , and  $\underline{F}(t)$  is a  $M \times 1$  vector composed of the muscle forces. Specific moment arm values for a 2-DOF-arm model are given in Appendix B.

#### *Equivalent Muscle Dynamics*

In our model it is assumed, that the dynamic relation between the control signal  $u_i(t)$  and the muscular force  $F_i(t)$ , is given by a simple first order low pass filter:

$$u_i(t) = F_i(t) + \alpha F_i'(t), \text{ s.t. } u_i(t) \geq 0 \quad i = 1, \dots, M, \text{ or}$$

$$(6) \quad \underline{U}(t) = \underline{F}(t) + \alpha \frac{d\underline{F}(t)}{dt}, \text{ s.t. } \underline{U}(t) \geq 0,$$

where  $\underline{U}(t)$  is a  $M \times 1$  vector of the MCSs  $u_i(t)$ .

It should be noted that in our model, MCSs describe the *population* activity of cortical neurons contributing to the input of motor neuron pools. This population activity is neither an EMG signal nor does it represent motor neuron activity, though it is closely related to them. In particular, the relation between muscular force and its control signal is not identical with the dynamics of an anatomical muscle (or with a combined action of several anatomical muscles, in case of a simplified arm model), since the dynamics of equivalent

muscles includes the influence of the spinal cord as well. Thereby we have used a relatively large value of the decay coefficient  $\alpha$ . The value of the decay coefficient was estimated to be 200 ms, leading to a good fit with experimental results. This relatively large value, accounts for the overall response time of the spinal cord, muscle excitation and muscle activation. Additionally, we've tested the sensitivity of the model's predictions to the value of  $\alpha$ , and show that the general patterns predicted by the model are robust over a wide range of values of  $\alpha$  - see Results.

#### *From Single Neuron Activities to MCS*

In our model each cortical muscle related neuron contributes to one of the MCSs. We assume that the control signal is given by a sum of delayed neural activities. Specifically,

$$(7) \quad u_i(t) = \sum_{j=1}^{N_i} w_{i,j} n_{i,j}(t - d_{i,j}) \quad , \text{ where } n_{i,j}(t - d_{i,j}) \geq 0 \quad j = 1, 2, \dots, N_i \quad i = 1, 2, \dots, M \quad ,$$

where  $u_i(t)$  is the control signal corresponding to the  $i$ -th equivalent muscle,  $n_{i,j}(t)$  is the control signal (e.g., firing rate) corresponding to the  $j$ -th neuron contributing to the  $i$ -th equivalent muscle,  $w_{i,j}$  is its weight, and  $d_{i,j}$  is the latency of the neuron, i.e. the time it takes its output to reach the motor neurons. We further assume that the latencies  $d_{i,j}$  are distributed uniformly in the range of [50ms, 100ms], as the typical delay between M1 neural activity and muscle activity is 50-100 ms (Morrow and Miller, 2003). These delays are long compared with the conduction times (about 10ms), due to inward currents in the motor-neurons (Morrow and Miller, 2003). The neural signals  $\{n_{i,j}(t - d_{i,j})\}_{j=1}^{N_i}$  are computed in Appendix A, for any fixed weights and delays, and are given by (11).

#### *Redundancy Resolution*

The motor system is highly redundant (Bernstein, 1967). Yet, arm movements are highly stereotypical under a large variety of experimental conditions, and generally vary little within and between subjects.

Furthermore, variability tends to decrease with practice. Thus, the redundancy of the motor system is resolved in a principled manner.

One may derive a criterion for redundancy resolution in several ways. One possible approach is based on the engineering principle of optimal control (Chow and Jacobson, 1971; Engelbrecht, 2001; Pandy, 2001), which proposes that the system operates by optimizing a given cost function under the appropriate constraints. A second possible approach is to simply postulate an empirical redundancy resolution rule, verifying that it indeed explains and predicts observed phenomena. Finally, one may use self-organizing neural network models, whereby the redundancy is resolved by the dynamics of these systems. While each of these approaches possesses its merit, we have chosen to base our derivation on optimal control theory, which fits in nicely with an evolutionary view of the nervous system.

However, such an approach may pose some difficulties. The fact that the brain tries to reduce some costs and converges to some solution does not necessarily imply that it always reaches the optimal solution. The question arises as to whether biological neural networks actually solve optimization problems; for discussions see (Carpenter et. al., 1987). The organization of the brain may impose further constraints on the motor plan. The studies of Morasso (1981), Shadmehr and Mussa-Ivaldi (1994) and Torres and Andersen (2006) suggest that the brain employs an independent path plan, and thus restricts the possible muscle control signals. Similarly, motor primitives (Bizzi et al., 1991) may impose restrictions on the possible control signals. Yet, the motor planning restrictions may be included in the constraints of the optimal control problem. For example, the stochastic optimal feedback control model of Burdet and Milner (1998) incorporates motor primitives as constraints.

We believe that the three redundancy resolution approaches alluded to above are complementary, rather than contradictory. The empirical approach focuses on the question "What", the optimal control theory approach focuses on the question "Why", and the neural network approach deals with the question "How".

In the present study, we use optimal control theory, based on simple optimality criteria. The redundancy of the system is resolved in two stages. First, we compute the MCSs according to a muscle optimization criterion and then compute how each MCS is divided between different neurons, according to a neuron-based optimization criterion.

#### *Optimization Criterion for the MCSs*

A natural question that arises pertains to the cost function used. We can get a qualitative general answer to this question from observations of motor learning processes. For example, the studies of (Burdet et. al., 2001; Franklin et. al., 2003) show, that when a human subject learns to reach a target through an unstable force field, two phenomena occur during the learning period. First, the percentage of successful trials increases and second, the EMG, and concomitantly, energy consumption, decreases. Such observations are supported by the clear evolutionary advantage of improving both task performance and saving energy. Furthermore, each of these two tendencies cannot be explained as a result of the other one. For example, unless a trained task requires high accuracy, the brain will not employ significant co-activation in order to achieve higher accuracy (Hogan 84, Osu et al., 2004). The conclusion is that the cost function should combine both task performance and energy consumption (Hogan 1984; Miyamoto et. al., 2004).

In order to resolve the MCS redundancy, we have used a quadratic optimization criterion, given by

$$(8) \quad \underline{U}(t) = \arg \min_{t_0 \leq t \leq t_f} \frac{1}{2} \int_{t_0}^{t_f} \underline{U}^T(t) \underline{U}(t) dt ,$$

where  $t_0$  and  $t_f$  are the initial and final trajectory times. The simplifying factor of  $1/2$  has no influence on the solution.

Our choice of a quadratic optimality criterion is based on the following reasoning.

- 1) A squared neural control input is a simplified model of muscle energy consumption. Under isometric force conditions and up to 30 percent of maximum contraction, the metabolic power consumption of the muscle is proportional to the squared neural control input (Hogan, 1984).

- 2) Some studies have demonstrated the predictive capability of such a criterion. For example, the study of Bolhuis & Gielen (1999) demonstrated that a quadratic cost function successfully predicted EMG activity of arm muscles under conditions of isometric static force.
- 3) As mentioned above, in general, the cost function combines both task performance and energy consumption. In the present case, we assume well-trained tasks, which do not require the hand to achieve high accuracy or to retain stability against significant perturbations. In this case, using a minimum energy criterion is reasonable.

### *Optimization Criterion for Neural Activities*

We assume that neural activity at the level of the single cell is selected in a way that minimizes the randomness of the muscle control signal. Our motivation here is that single neurons are noisy elements, and noise reduction through averaging may be one reason for using a large number of neurons for controlling the muscles. We assume here an optimization criterion, which is related to a measure of MCS stochasticity. The criterion is based on a very general assumption regarding the way in which a single neuron contributes to the stochasticity measure of the muscle control signal. In particular, we assume that

$$(9) \quad \left\{ n_{i,j}(t - d_{i,j}) \right\}_{j=1}^{N_i} = \arg \min \int_{t_0}^{t_f} \sum_{j=1}^{N_i} f(w_{i,j} n_{i,j}(t - d_{i,j})) dt \quad i = 1, 2, \dots, M \quad ,$$

where  $f(x)$  is a strictly convex function. Examples for functions that obey the above restriction are  $f(x) = x^r$  where  $r > 1$ . A function that does not obey this restriction is  $f(x) = x$ . The restriction on  $f(x)$  ensures that the optimality criterion will impose a single solution. The exact shape of  $f(x)$  does not influence the solution – see Appendix A. As a specific example, we may assume that  $f(x)$  is the variance of  $x$ .

Next, we present the full optimization problem leading to the computation of the MCS and the neural activity.

*The complete Optimal Control Problem*

$$\min_{\substack{\underline{U}(t) \\ t_0 \leq t \leq t_f}} \frac{1}{2} \int_{t_0}^{t_f} \underline{U}^T(t) \underline{U}(t) dt$$

$$\text{s.t.} \quad (10a) \quad \underline{U}(t) = \underline{F}(t) + \alpha \frac{d\underline{F}(t)}{dt}$$

$$(10b) \quad \underline{R}^T \underline{F}(t) - \underline{\tau}(t) = 0$$

$$(10c) \quad \underline{U}(t) \geq 0$$

Then for each  $i = 1, 2, \dots, M$

$$\min_{\substack{\{n_{i,j}(t-d_{i,j})\}_{j=1}^{N_i} \\ t_0 \leq t \leq t_f}} \int_{t_0}^{t_f} \sum_{j=1}^{N_i} f(w_{i,j} n_{i,j}(t-d_{i,j})) dt$$

$$\text{s.t.} \quad (10d) \quad \sum_{j=1}^{N_i} w_{i,j} n_{i,j}(t-d_{i,j}) - u_i(t) = 0$$

$$(10e) \quad n_{i,j}(t-d_{i,j}) \geq 0 \quad j = 1, 2, \dots, N_i \quad .$$

*Solution*

The above optimal control problem is solved analytically in Appendix A, leading to the optimal neural activity

$$(11a) \quad n_{i,j}(t-d_{i,j}) = a_{i,j} u_i(t) \quad j = 1, 2, \dots, N_i \quad i = 1, 2, \dots, M$$

where the constants  $a_{i,j}$  are computed in Appendix A. The optimal MCS is given by

$$(11b) \quad \underline{U}(t) = \left[ \underline{R} \left( \underline{R}^{(k)T} \underline{R}^{(k)} \right)^{-1} \left( \underline{\tau}(t) + \alpha \frac{d\underline{\tau}(t)}{dt} \right) \right]_+$$

where the constant matrix  $\underline{R}^{(k)}$  contains a subset of the rows of  $\underline{R}$  as explained in Appendix A.

For an isometric task (see Appendix A), the MCSs are given by

$$(11c) \quad \underline{\underline{U}}(t) = \left[ \underline{\underline{R}} \left( \underline{\underline{R}}^{(k)T} \underline{\underline{R}}^{(k)} \right)^{-1} \underline{\underline{J}}^T(\underline{\underline{\theta}}) \left( F(t) + \alpha \frac{F(t)}{dt} \right) \underline{\underline{D}}(\varphi) \right]_+ .$$

Under the assumption of generalized symmetry (see Appendix A for details) a simplified expression results,

$$u_i(t) = \left[ \left( F(t) + \alpha F'(t) \right) r_i(\underline{\underline{\theta}}) \cos(\varphi - \varphi_i(\underline{\underline{\theta}})) \right]_+, \quad i = 1, 2, \dots, M \quad ,$$

$$\text{where } r_i(\underline{\underline{\theta}}) = \sqrt{C_{i,1}^2 + C_{i,2}^2} \quad \varphi_i(\underline{\underline{\theta}}) = \text{tg}^{-1} \left( \frac{C_{i,2}}{C_{i,1}} \right) \quad \text{and } \underline{\underline{C}}(\underline{\underline{\theta}}) = \underline{\underline{R}} \left( \underline{\underline{R}}^{(k)T} \underline{\underline{R}}^{(k)} \right)^{-1} \underline{\underline{J}}^T(\underline{\underline{\theta}}) .$$

The solution flow chart is summarized by Fig. 1b. The variables appearing in the model are summarized in Table 1. A detailed solution with specific parameters and arm configuration for the 2-DOF-arm model is given in Appendix B.

### *Experimental Setup*

We refer to a variety of experimental results published in the literature and present comparative model results. In particular, we provide a detailed comparison of our model's predictions with the experimental results of (Sergio and Kalaska, 1998; Sergio et al., 2005). Our comparisons to the experimental results used only published data and figures.

We describe briefly the experimental setup of (Sergio and Kalaska, 1998; Sergio et al., 2005). Two juvenile rhesus monkeys (a.k.a. *Macaca mulatta*) were trained to perform an isometric task and a movement task. The activity of single cells in the caudal part of M1 was recorded during both tasks. A neuron was selected if it was related to movements of the shoulder and/or the elbow but not to more distal joints, and it displayed directional tuning in at least one of the tasks. Most neurons were related to the shoulder and shoulder girdle, with a smaller number related to the elbow. The recorded neurons were in the caudal part of M1 of three hemispheres from the two monkeys (71 and 17 cells from the left and right hemispheres of monkey A, 44 cells from the right hemisphere of monkey B). Attempts were made to record neurons from all cortical layers but the need for stable isolation over long periods of time led to a bias toward neurons in

intermediate cortical layers. The set of recorded neurons included 132 cells. A particularly interesting aspect of the experiment is that the activity of the *same* neurons was recorded for the two different tasks (isometric and movement), enabling a detailed study of the (considerable!) change of activity of the same cell between tasks.

In an isometric task, the subject retains a fixed end-point position in the face of an external force field. The dynamic profile of absolute force is the same in all trials, while force direction changes between trials. The force in this case was assumed to be  $\underline{F}^{(ex)}(t) = F(t) [\cos(\varphi) \quad \sin(\varphi) \quad 0]^T = F(t) \underline{D}(\varphi)$ . The monkey held a static handle during 1-3 seconds (center hold time), and was then required to exert a ramp force of 1.5N in one of eight directions. Force directions were spaced at 45° intervals, starting at 0°. We've estimated the shape of the force ramp, according to graph 1A in Sergio and Kalaska (1998), as a second order spline with rise duration of 150ms. The monkey was required to produce a force trajectory, which was confined to a horizontal plane (a significant vertical force resulted in an error). The handle was positioned in front of the monkey while hand location was at the midline, 20cm in front of the sternum.

In the movement task the monkey was required to push a load of 1.3kg by 8cm. Movement duration was about 0.6sec, and the directions of movement were spaced at 45° intervals, starting at 0°. Since we did not have experimental data about the hand trajectory in the movement task, we assumed a minimum jerk trajectory (see Appendix B). The inertial force during movement was calculated according to the relation  $F = ma$ . After movement the monkey was required to exert a force of about 1N against the pendulum. We've assumed that the force profile following the movement period is described by  $F(t) = 1 - ae^{-bt}$ , where  $a$  and  $b$  are chosen in a way that retains the continuity of the force and its first derivative at the end of movement.

## Results

### Intuition

We provide here a brief summary of the model's predictions, and their relation to the model assumptions described in Methods. We discuss both the directional behavior and the response through time.

A *temporal tuning function* maps a time dependent external force or movement direction into a related signal, e.g., the temporal firing rate of an M1 cell. A weighted sum of several cosine functions is a cosine function (i.e.  $a \cos(\theta - \alpha) + b \cos(\theta - \beta) = c \cos(\theta - \gamma)$ ). In the isometric force task, each one of the external force components changes with direction as a cosine function and therefore, a linear relationship between end point force and the neural activity implies cosine tuning. Under isometric conditions, the relation between endpoint force and joint torques is linear (Equation 3). However, due to the muscle unidirectionality (Equation 6), the relation between the MCS and joint torques is linear for positive values and zero otherwise (Equations 11b). Therefore, the tuning function, predicted by the model under isometric conditions, is a truncated cosine rather than a full cosine.

The *preferred direction* (PD) is the direction corresponding to the peak of the tuning function. Since the linear relation between endpoint force and joint torques depends on the Jacobian (Equation 3), the PD changes with arm posture.

The truncated cosine was obtained due to the linear relation between endpoint force and joint torques (Equation 3) under isometric conditions. Yet, in the movement task, the non-linearity of arm dynamics (Equation 4) leads to non-cosine tuning at certain periods of the movement task.

Let us assume that the time response of the control signal simply follows the joint torques. In the isometric task we would expect a positive or negative step response, and in the movement task we would expect a positive step followed by negative one, or a negative step followed by positive one (depending on

movement direction). Since muscles are unidirectional (Equation 6), negative pulses are impossible and negative torques are produced by the antagonist muscles alone. Taking this consideration into account we would expect a non-symmetric response. Thus, in the isometric task we would expect a step response or no response, depending on force direction. In the movement task we would expect a pulse-pause response or a pause-pulse response, depending on movement direction. We denote the latter pattern as bi-phasic. However, we should take into account the finite time response of the equivalent muscle, expressed by the decay coefficient (Equation 6). Due to the finite time response, we obtain a pulse-step rather than a step response in the isometric task, and a tri-phasic rather than a bi-phasic response in the movement task. We elaborate on these issues in the following sections.

### **Isometric Task: Directional Behavior**

In this section we test different properties of the predicted neural command signal, given by Equation (11).

#### *Tuning Function*

Equation (11c) shows that the shape of the resulting tuning function of all MCSs is half cosine. If gravity is considered, the tuning function is a truncated cosine with a width, which is wider or narrower than  $180^\circ$  - see Appendix A. An example of the tuning functions for the 2-DOF-arm model is given in Fig. 3a. From equation (11a), we expect that the tuning function of a single neuron should also be a truncated cosine function. Such a tuning function is narrower than a full cosine. How does the prediction of a narrow tuning function match the experimental data? Fig. 3d shows an example of a representative neuron from Sergio et al. (1998, 2005), for which the width of the tuning function is approximately  $180^\circ$ . The tuning functions of 51% of the cells in Amirkian and Georgopoulos (2000) were considerably narrower than  $360^\circ$ . According to Paninski et al. (2004), about a third of the neurons have narrow tuning function.

#### *PDs*

While different MCSs have tuning functions with similar shapes, they are distinguished by their PDs. For example, the PDs in the 2-DOF-arm model are  $355^\circ$  for the shoulder flexor,  $30^\circ$  for the bi-joint flexor,  $87^\circ$  for the elbow flexor,  $175^\circ$  for the shoulder extensor,  $210^\circ$  for the bi-joint extensor and  $267^\circ$  for the elbow extensor – see Fig. 3b. In fact, the PD of each MCS is in one of two opposite directions. For example, the PD of  $u_1(t)$  is  $355^\circ$  or  $175^\circ$  depending on the sign of the expression  $F(t) + \alpha F'(t)$ . Thus, the PD of the control signal is *reversed* during the task whenever the expression  $F(t) + \alpha F'(t)$  changes its sign. We will address this phenomenon in the movement task section. Elsewhere, we refer by PD to the PD given that  $F(t) + \alpha F'(t) > 0$ .

#### *Hand Location and Arm Posture Dependence of Directional Tuning*

According to Equation (11c), the PD depends on hand position and hand location through the Jacobian. Fig. 3c shows an example of PD dependence on hand location in the 2-DOF-arm. Systematic changes in directional tuning due to hand location or arm posture have been observed in several studies (Caminiti et al. 1990; Lacquaniti et al. 1995; Scott and Kalaska 1997; Sergio and Kalaska 1997, 2003; Ajemian et al. 2000; Hocherman and Wise 1991). According to Equation (11b) of our model, neural directionality is defined in  $(\underline{\tau}(t) + \alpha \underline{\tau}'(t))$ -space. We elaborate on this issue in the Discussion.

#### *Isometric Task: Dynamic Behavior*

##### *Average Response*

In the isometric task, different tuning functions differ only in their PD. Therefore, according to equation (11c), the neural activity, aligned to the neuron's PD, of all cortical muscle related neurons is given by:

$$(12) \quad Q(t) \propto \left[ \left( F(t) + \alpha \frac{dF(t)}{dt} \right) \cos(\varphi_{CM}) \right]_+$$

where  $Q(t)$  is the aligned neural response and  $\varphi_{CM}$  is the force direction relative to the neuron's PD. This result is very robust, since it depends only on a single parameter -  $\alpha$ . Furthermore, this result *does not* depend on the specific arm model used.

Equation (12) can also be used to describe the average of aligned neural responses, where the average is taken over many neurons. In practice, such averaging procedures suffer from two problems. First, different neurons have different latencies (Equation 7). A possible way to resolve this problem is to estimate the latency of each neuron and align its response with respect to time before averaging. A neuron's latency can be estimated by computing the cross-correlation between its activity and the EMG signals (Morrow and Miller, 2003). However, since the experimental data we've examined is based on a simple average, we had to compensate for the effect of different latencies by smoothing the predicted averaged response. We've smoothed the predicted averaged response by assuming that the latencies are distributed uniformly in the range of [50ms, 100ms].

Second, in the calculation of the experimental averaged response, each neuron's response is not exactly aligned to its PD, since in practice the PDs are given within a resolution of  $45^\circ$ . This low resolution creates a smoothness effect in the direction axis as well. In order to compensate for this we've smoothed the predicted averaged response, by assuming that the directionality alignment is distributed uniformly in the range of  $[-22.5^\circ, 22.5^\circ]$ .

#### *Predicted Control Signal*

If the control signal were defined merely relative to the muscle force, we would get a signal with similar shape to the muscle force profile. However, the control signal is also related to the first derivative of the muscle force (see Eq. 6). Therefore, instead of obtaining a step response, we get a pulse step response – see Fig. 4. The pulse-step result is robust with respect to a wide range of values of the force derivative coefficient ( $\alpha$ ) as shown in Fig. 4c. The value of  $\alpha$  only determines the relative height of the pulse in the pulse-step response.

In order to obtain an averaged response, the above profile is multiplied by a truncated cosine as described by Equation (12). As explained above, the averaged response is smoothed in order to account for the effects of the simple averaging. Recall that Equation (12) is independent of the arm model and therefore the comparison with Sergio et al. (2005) is appropriate. The averaged response in Sergio et al. (2005) was generated from those neurons that were directionally tuned during target hold time, using the PD from that epoch. The good qualitative match between the experiment and model can be clearly observed in Fig. 5.

### *Interpretation*

The population vector is defined as the sum of neuronal firing rates (relative to each cell baseline) multiplied by each neuron's PD unit vector (Georgopoulos et al., 1983). The population vector has been used in order to estimate output variables based on neural activity. In the experiment of Sergio et al. (2005) the population vector significantly deviates from the force direction, as shown in Fig. 11 in Sergio et al. (2005). The description of the population activity as a control signal has two advantages over the description of the population activity by a population vector of hand force. First, the control signal can be approximated by a simple average. Second, the agreement between the MCS and the averaged neural activity is better than the agreement of the population vector with the external force. Indeed, modern extraction algorithms (e.g., Salinas and Abbott, 1994; Taylor et al., 2002; Wu et al., 2004; Shpigelman et al., 2005) significantly improve the accuracy of the simple population vector. However, such techniques are much more complex than the simple average we have used. This does not reduce the importance of such algorithms for BMI applications. However, in the above case, “the population codes a MCS”, is the preferable interpretation of the population activity, since it is the simplest interpretation that matches the experimental results.

### *Single Cell Activity*

The predicted single cell response is proportional to the MCS response (see equation 11), i.e. a pulse step response multiplied by a half cosine tuning function. Notice that for the single cell, there is no need to apply a smoothing procedure and therefore Equation (12) was used without further processing. In the experiment of Sergio and Kalaska (1998) 28% of the cells demonstrated a dynamic response similar to the response predicted by our model. See Fig. 6 for a comparison between this subset of neurons and the predicted response. The time response of most other cells was similar to part of the predicted response: 36% of the cells displayed a step response at their PD and 29.3% displayed a pulse response. 6.7% of the cells were unclassifiable. There are several possible reasons why the predictions of our model with respect to single cell activity apply only to a subset of the neurons reported on in the experiments. We elaborate on these in the discussion.

### ***Movement Task***

#### *Isometric Force Approximation*

Let us assume an isometric force experiment, in which the force profile is given by  $F(t) = m \cdot a(t)$  where  $m$  is the mass of the external load and  $a(t)$  is the acceleration in the movement experiment. We refer to this approximation as the *isometric force approximation*. There are two differences between this approximation and an accurate description of arm mechanics:

- (a) Hand position, and consequently the Jacobian, changes during movement. Yet, our simulation with the 2-DOF-arm model and 8 cm movement distance shows that the assumption of fixed hand position has a minor effect on the tuning function.
- (b) Besides moving the load, the muscles also need to move the arm itself. This effect is calculated using the dynamics (Equation 4). We discuss the effect of this component later. In the meantime we assume that this effect is insignificant.

Under these simplifying assumptions we can calculate the control signal's joint torques in a similar way to the isometric task.

### *Tri-Phasic Response*

Fig. 7a and 7b show graphs of  $F(t)$  and of  $F(t) + \alpha F'(t)$ , for the isometric force approximation of the movement task. As shown, there is an important difference between the movement task and the isometric task with force ramp profile. Unlike the force ramp profile scenario, the expression  $F(t) + \alpha F'(t)$  is not always positive. The profile of  $F(t) + \alpha F'(t)$  is tri-phasic, where the first phase is positive, the second is negative and the third is positive again. We refer to this type of response as tri-phasic as it relates to a known phenomenon, in which the activation period of one muscle is followed by an activation period of the antagonistic muscle, followed by a further activation period of the first muscle. We refer to the transition times between the first and the second phases and between the second and third phases as *transition times*. If we examine two antagonistic muscles in the 2-DOF-arm model, for example, the shoulder flexor and the shoulder extensor, it is clear that the predicted pattern is tri-phasic. The tri-phasic response is a pattern of flexor-extensor-flexor, or alternatively extensor-flexor-extensor, depending on the movement direction. Note that the brain would not employ a tri-phasic pattern if not for the finite time response of the equivalent muscles. When the neural input to a muscle ceases, the muscular force does not vanish immediately, since it has some decay period. In order to change the muscular force rapidly enough, the antagonistic muscle should be activated, while the agonist muscle is still active – see Fig. 7c.

Fig. 7d and 7e show that the tri-phasic response is robust, as it occurs for all values of  $\alpha$ . The value of  $\alpha$  only determines certain details of the shape of the curve. The first pulse gets narrower with the increase of  $\alpha$ , the second pulse shifts to the left and the third pulse broadens with the increase of  $\alpha$ . To understand the influence of  $\alpha$ , notice that the force profile (Fig. 7a) is quite similar to a sine wave. Therefore, the 'phase shift' of  $F(t) + \alpha F'(t)$  (Fig. 7b) becomes larger with the increase of  $\alpha$ .

### *Population Activity*

Fig. 8 presents a comparison of the experimental results with the model's prediction. The simulation is based on Equation (12), as we used the isometric force approximation. Recall that Equation (12) is *independent of the arm model* and therefore the comparison with Sergio et al. (2005) is appropriate. The average response in Sergio et al. (2005) was generated for those neurons that were directionally tuned during target hold time, using the PD from that epoch. As can be seen in Fig. 8, the temporal behavior of the neural signal predicted by the model corresponds to the experimental results. Particularly important is the fact that the results for both the isometric (Fig. 5) and the movement (Fig. 8) tasks reproduce the qualitative shift in neural activity between the two tasks.

### *Single Cell Activity*

Fig. 9 displays a comparison between a subset of neurons in the experiment and the predicted response. For the simulation, Equation (12) was used without smoothing. In the experiment 87.5% of the cells, displaying step or pulse-step response in the isometric task (56% out of all the cells) displayed the burst-pause-burst response in their PD (Fig. 9a) as predicted by the model (Fig. 9b). Most of these cells (78% or 44% out of all cells), as well as part of the cells in the remaining group, displayed the predicted response of pause-burst-pause in the opposite direction, as shown in Fig. 9a and 9b. 45.4% of the cells, exhibiting a pulse response in the isometric task (13% out of all the cells), displayed the burst-pause-burst response in their PD. Many of these cells displayed the response of pause-burst-pause in the opposite direction. Other neurons in the movement task displayed pulse response (20%), step response (13%), pulse-step response (4%) and the rest were unclassified. Similarly to the single-cell dynamic response for the isometric task, the agreement with our predictions is partial though significant. We elaborate on this issue in the Discussion.

### *PD Reversal*

According to Results / Isometric task: Directional Behavior / PDs, the PD of the control signal is reversed each time the expression  $F(t) + \alpha F'(t)$  changes its sign. Therefore, in movement tasks, the PD of the control signals is reversed during the second phase. According to the model, we expect to see such a phenomenon at the level of the single cell as well. Fig. 10 shows that this prediction matches the experimental data. The graph of Sergio et al. (2005) was generated from the cell activity shown in Fig. 9, which represents 44% of the cells. Note that the PD goes through two reversals during the movement task, as expected from the model.

### *Non Cosine Behavior*

The control signal in our model can be decomposed into two components. One component is related to arm movement and the second is related to the load movement. The isometric force approximation is based on the assumption that the torque needed to move the arm is small compared with the torque needed to move the load. This assumption holds only when the expression  $F(t) + \alpha F'(t)$  is significant. However, when the load is insignificant and/or during periods around the transition times, the isometric force approximation is poor. The component related to arm movement is significant during periods around the transition times, since  $F(t) + \alpha F'(t) \approx 0$ . In the experimental setup we've examined the load was significant. However, we still expect the isometric force approximation to be poor around the transition times. During these periods the non-linear arm dynamics becomes more significant. Consequently, half cosine tuning is not expected anymore.

In order to simulate this phenomenon, we cannot use the general equation for the isometric task (Equation 12), as the calculations in this case depend on the arm model. We need to calculate the control signals according to Equation (11b). However, the arm in this experiment was allowed to move in 3-D space, while we do not have data about the monkey's arm moments for a 4-DOF model. Therefore, we have studied this phenomenon using the 2-DOF-arm model, as described in Appendix B, assuming that qualitatively, the kind of effect of dynamic non-linearity around transition times would be similar for the 2-DOF and the 4-DOF models. Our simulations (with the 2-DOF model) show that during these periods the tuning

function becomes wider and loses its cosine shape - an example of a bimodal tuning function can be seen in Fig. 10c. The non-cosine prediction is in agreement with the experimental results shown in Fig. 10a. During periods around the transition times, cell activity was not directionally tuned (time windows represented by circles).

## Discussion

We have presented a mechanistically explicit modeling approach based upon the following principles:

- 1) It is possible to attribute functional meaning to neural activity in the motor areas in the brain.
- 2) Understanding the spinal cord and the limb biomechanics is essential to interpreting the motor control signals descending from the brain to the spinal cord. In particular, the motor cortex control signals are related to endpoint variables through dynamic models.
- 3) The redundancy of the control signals can be resolved using optimal control theory.
- 4) Neural activity characteristics, such as tuning functions, PDs and coordinate systems, can be derived within a general theoretical framework.

Based on this modeling approach, we have presented a model, which explains muscle related neural activity in the primary motor cortex. The model has demonstrated good agreement with a variety of experimental results.

The model successfully predicted the temporal population activity in the isometric and movement tasks (pulse-step, tri-phasic), and for different force or movement directions (truncated cosine), as well as the qualitative nature of the transition between the two tasks. There are a few differences between the population predicted responses and the experimental results. The peaks in the experiment are wider and continue beyond the force ramp / movement duration, and the tuning function in the experiment is somewhat wider. Additionally, there is a ~10 spikes/s ground level in the experiment.

The predictions of the time responses of the single cell partially agree with the experimental results. A subset of the cells (28% in the isometric task, 44% in the movement task) displayed close similarity with the predicted response. Most other cells displayed similarity only to part of the response. Comparing population and single cell predictions, a subset of the single cells displayed better similarity than the population response (narrow peaks, no ground level), while others displayed less similarity than the population response (e.g., single-cell pulse response in the movement task).

The gaps between model and experiment are possibly due to the model's simplifications and/or because only part of the neurons examined in Sergio and Kalaska (2005) were muscle related cells. It is difficult to determine which of these two reasons is more important, as we do not know which of the cells were muscle-related. In order to better examine models of neural activity in M1, one should use recorded activity of neurons with similar connectivity, i.e. the connectivity of the measured neurons should be identified.

The prediction of single cell tuning functions is supported by experimental results. The model successfully predicts the half cosine tuning function in Sergio and Kalaska (1998). This prediction also agrees with Amirikian and Georgopoulos (2000) and with Paninski et al. (2004) showing that a significant fraction of the primary motor cortex neurons have narrow tuning functions. Interestingly, the analysis of Paninski et al. (2004) shows that narrowness of the tuning function correlates with the information about hand trajectory conveyed by the cell. The model also successfully predicted non-cosine tuning-functions around the transitions times of the movement task.

While tuning functions and PDs do not possess an intrinsic functional meaning in the context of our model, we've calculated them in order to compare our results with published experimental data. The model predicts the dependency of the PD on arm posture and on hand location, as well as the two reversals of the PD during the movement task.

In addition to explaining known results, one may try to test the model's predictions in new situations. For example, our simulations show that the phenomenon of unusual tuning functions around transition times becomes more apparent as the load becomes lighter. The reason for this is the non-linear nature of arm dynamics, which becomes more significant at small loads, where the isometric force approximation is poor. This prediction has not yet been tested experimentally.

The model's relative simplicity and analytic tractability support a causal explanation of how each of the plant's properties influences the overall behavior. Such an explanation was given in Results.

Our model is aimed at predicting the behavior of muscle related cells. Yet, many M1 neurons are not muscle related cells (Alexander and Crutcher, 1990; Crutcher and Alexander, 1990; Kakei et al., 1999; Ashe 2005). Thus, it is possible, that the neural activity of other neurons in M1 have very different interpretations, such as movement direction. One possible interpretation of cosine tuning (Georgopoulos et al., 1982) and of the population vector (Georgopoulos et al., 1983) is that M1 employs a coding scheme based on external space directions. However, correlations with high-level parameters are not sufficient to prove high-level representation. Cosine tuning and the existence of a population vector are determined by very general necessary and sufficient conditions, rather than by any intrinsically coded coordinate system (Mussa-Ivaldi, 1988; Sanger, 1994). However, the analysis of Mussa-Ivaldi (1988) and of Sanger (1994) does not exclude the possibility of direction coding. It just shows that the cosine tuning and the population vector are not sufficient to determine whether neurons code directions in external coordinates or in some intrinsic coordinate system. In order to better model the neural activity, further information is needed. Indeed, dissociation experiments (e.g., Evarts, 1968, Thach, 1978, Crutcher and Alexander, 1990, Scott and Kalaska, 1997) provide further information, which enables one to distinguish between different interpretations of neural activity. Interestingly, the early dissociation experiment of Evarts (1968) showed that the discharge frequency of the majority of pyramidal tract neurons was related primarily to the force and to the force derivative and was only secondarily related to the direction of displacement.

Currently, it is known that neural coding in the motor cortex is much more complex than described by cosine tuning and the population vector (Johnson et al., 2001). Neurons in M1 do not possess a single fixed PD. The PD depends on external variables (such as force or velocity) with which the neuron is correlated. The correlations change for different tasks, and also as a function of time within a *single* task. Many of the tuning functions in M1 are narrow, asymmetric and sometimes bi-modal (Amirikian and Georgopoulos, 2000), and the population vector may deviate from extrinsic variables (Scott et al., 2001). Yet, the question of distinguishing between different interpretations of neural activity is always relevant. Interpretations of neural activity are in fact models. Therefore, it is possible to choose between different interpretations on the basis of the agreement with the experimental results, the simplicity of the model and the relative weight given to each of these two factors.

The study of Scott et al. (2001) shows that the population vector may deviate from extrinsic variables. Our study further shows in Results, that the MCS provides a better interpretation of the population activity reported in the experiments of Sergio et al. (2005) compared with the interpretation of end point force.

Observed PD changes, due to arm posture, can be explained by intrinsic coordinates, but not by external coordinates (Scott and Kalaska, 1997; Ajemian et al., 2000). Our model further suggests that such intrinsic coordinates do not necessarily follow simple mechanical expressions, such as joint angular velocities (Scott and Kalaska 1997; Ajemian et al. 2000) or torques (Scott and Kalaska 1997). In fact, the coordinates might be hard to guess without a physiological model, as even in our simplified model, the derived coordinates are composed of both joint torques and joint torque derivatives.

Several previous studies have presented models of neural activity in M1 and its functional interpretation. The early work of (Humphrey, 1972) described the relation between neural activity in the motor cortex and muscular torque by a dynamic linear model. We have followed the same approach. However, Humphrey (1972) addressed the forward control problem, while our model addresses the inverse control problem.

The model of Bullock and Grossberg (1988) and of Cisek et al. (1998) assumes that automatic processes convert the target position command and the movement's overall speed command into an arm trajectory. The focus of this model is quite different from ours. The model of Bullock and Grossberg (1988) and of Cisek et al. (1998) does not use optimal control theory in order to explain why the brain produces a certain control signal. On the other hand, it introduces a computational scheme for M1. Similarly, the model of Baraduc et al. (2001) focuses on how the motor cortex learns and computes control signals, using a neural network model. The neural network in this model transforms position in extrinsic coordinates into position in joint angle coordinates.

The model of Todorov (2000, 2002) describes the average neural activity of neurons with a certain PD by a population vector related to the external endpoint force, endpoint position, velocity and acceleration. We share with Todorov (2000, 2002) the general philosophy, according to which, understanding the spinal cord and the limb biomechanics is essential to interpreting the motor control signals descending from the brain to the spinal cord. However, our view and understanding of the spinal-muscular-skeletal system is very different from Todorov (2000, 2002). In fact, our model and Todorov (2000, 2002) are based on very different assumptions. Most importantly, the model used in Todorov (2000, 2002) does not contain muscle unidirectionality, muscle and spinal cord finite time response and realistic multi-joint mechanics (see, for example, Moran and Schwartz, 2000) - features which we find crucial for achieving qualitatively correct predictions. Due to the conceptual difference between the models, the predictions of the two approaches contradict each other, even in the simplest scenarios. For example, in an isometric force task the average neural activity predicted by Todorov (2000, 2002) differs from our prediction. First, the predicted tuning function in Todorov (2000, 2002) is a full cosine, while our model predicts a truncated cosine tuning function. Recall that both narrow and wide tuning functions are present in M1, however, muscle related cells have narrow tuning functions. Second, the response at the PD predicted by Todorov is a step, while our model predicts pulse-step response. The predictions of Todorov (2000, 2002) also differ from ours with respect to the movement task. For example, comparing Fig. 2C in Todorov (2002), and Fig. 9b in this work, with the results in Sergio and Kalaska, (1998, Fig. 1b) shows the current model provides a significantly better qualitative description – see comparison in Fig. 9.

Finally, the model of Neilson and Neilson (2005) uses a quadratic optimality criterion in order to resolve the redundancy of the muscle control signals. The model assumes known flexion and extension torques, which are used in linear equality constraints. Given that the flexion and extension torques are known, one can use this assumption with our general solution for the MCS, as this assumption simply doubles the number of linear equality constraints. Unlike our MCS model, the model of Neilson and Neilson (2005) is limited to static scenarios. Another important difference between this model and our model is that it does not include the inequality constraints due to muscle unidirectionality. In the case where all the predicted control signals are positive, the solution of this model is similar. In any other case, this model cannot be applied, due to negative control signals. Thus, our solution is more general.

While we have been able to demonstrate good agreement with experimental results, many open questions remain for future research, of which we mention a few. (i) Cortical neurons projecting to the spinal cord have further functionalities beyond providing input to the motor neuron pools. For example, projections to Ia-inhibitory inter-neurons enable the brain to regulate the gain of the reflex loop and thus change arm impedance. A more comprehensive model should take such connections into account. (ii) In order to extend the model's applicability and predictive power, a more realistic spinal-bio-mechanical model is needed. For example, in order to apply the model to tasks involving impedance control, it should take into account neural noise, control of the reflex loop gains, influence of the MCS amplitude on muscle stiffness and viscosity, and the dependence of arm moment on joint angles.

We should emphasize that this study provides but one step in a long journey towards the formidable task of constructing a unified controller-plant based model of the biological motor system. In general, the plant is very complex, the control policy is task dependent, and the diversity of tasks is large. Furthermore, the biomechanical system (Loeb et al., 2002) and the spinal cord (Burke, 2004) are not fully understood. In order to combine the plant model with a controller model, while incorporating appropriate optimality criteria, one needs solve the associated optimal control problem. In general, this computational problem is very difficult due to its high dimensionality and the inherent non-linearity and stochasticity. Finally, in

order to better test such models, the connectivity strengths of recorded neurons to different motor-neurons and inter-neurons should be identified. Clearly, the goal of achieving a full computational understanding of voluntary motor control is a long distance away. Nevertheless, we believe that the encouraging results of the simplified model we developed show that the task is not insurmountable.

## Appendix A

### General Solution

From Equations (10a) and (10b) we obtain

$$\underline{\underline{R}}^T \underline{U}(t) = \underline{\tau}(t) + \alpha \frac{d\underline{\tau}(t)}{dt} \quad t_0 \leq t \leq t_f .$$

Thus we have replaced Equations (10a) and (10b) with equality constraints which depend only on  $\underline{U}(t)$ .

Now, since the integrand of the cost function and the constraints depend only on  $\underline{U}(t)$ , the solution at a given time depends only on the integrand and the constraint at that particular time. Therefore, the optimal control problem can be replaced by the following optimization problem:

$$\min_{\underline{U}(t)} \frac{1}{2} \underline{U}^T(t) \underline{U}(t) \quad , \quad t_0 \leq t \leq t_f$$

$$\text{s.t.} \quad (i) \quad \underline{\underline{R}}^T \underline{U}(t) = \underline{\tau}(t) + \alpha \frac{d\underline{\tau}(t)}{dt} \quad (D \text{ equality constraints})$$

$$(ii) \quad \underline{U}(t) \geq 0 \quad (M \text{ inequality constraints}).$$

This problem can be solved using Lagrange multipliers – see, for example, Bryson (1999).

We denote Lagrange multipliers for the equality constraints by  $\lambda_j(t)$ ,  $j = 1, 2, \dots, D$ , and the Lagrange multipliers for the inequality constraints by  $\lambda'_i(t)$ ,  $i = 1, 2, \dots, M$ .

At the minimum the equality constraints  $\underline{\underline{R}}^T \underline{U}(t) = \underline{\tau}(t) + \alpha \frac{d\underline{\tau}(t)}{dt}$  are satisfied.

In addition, for each  $i = 1, 2, \dots, M$ , the solution satisfies one of the following two conditions:

(i) The minimum is on the boundary of the admissible region (so-called active constraints), and then

$$u_i(t) = 0 \ \& \ \lambda'_i(t) \geq 0 \ \& \ u_i(t) - \sum_{j=1}^D \lambda_j(t) R_{ij} - \lambda'_i(t) = 0.$$

(ii) The minimum is inside the admissible region (so-called inactive constraints), and then

$$u_i(t) > 0 \ \& \ \lambda'_i(t) = 0 \ \& \ u_i(t) - \sum_{j=1}^D \lambda_j(t) R_{ij} = 0.$$

Thus, either

$$(i) \ u_i(t) = 0 \ \text{and} \ \sum_{j=1}^D \lambda_j(t) R_{ij} \leq 0, \ \text{or}$$

$$(ii) \ u_i(t) = \sum_{j=1}^D \lambda_j(t) R_{ij} \ \text{and} \ \sum_{j=1}^D \lambda_j(t) R_{ij} > 0.$$

We conclude that

$$\underline{U}(t) = \left[ \underline{R} \underline{\lambda}(t) \right]_+, \ \text{where} \ \underline{\lambda}(t) = [\lambda_1(t), \lambda_2(t), \dots, \lambda_D(t)]^T, \ \text{and where} \ [x]_+ = x \ \text{if} \ x \geq 0 \ \text{and}$$

zero otherwise.

Therefore, the D equality constraints become

$$\underline{R}^T \left[ \underline{R} \underline{\lambda}(t) \right]_+ = \underline{\tau}(t) + \alpha \frac{d\underline{\tau}(t)}{dt}.$$

$$\underline{U}(t) = \left[ \underline{R} \underline{\lambda}(t) \right]_+ \ \text{and therefore, the set of equations} \ \underline{R} \underline{\lambda}(t) = 0 \ \text{divides the space} \ \Lambda, \ \text{spanned by}$$

$\underline{\lambda}(t)$ , into regions  $\Lambda^{(k)}, k = 1, 2, \dots, K$ . For each region  $\Lambda^{(k)}$  there is a unique group of active muscle

indices  $m_k$ , for which  $u_i(t) > 0, i \in m_k$ . More precisely

$$u_i(t) = \begin{cases} \sum_{j=1}^D \lambda_j(t) R_{ij} > 0 & i \in m_k \\ 0 & i \notin m_k \end{cases}.$$

Since  $\underline{\underline{R}}^T \left[ \underline{\underline{R}} \underline{\lambda}(t) \right]_+ = \underline{\tau}(t) + \alpha \frac{d\underline{\tau}(t)}{dt}$  is a continuous transformation from  $\Lambda$ -space to

$\left( \underline{\tau}(t) + \alpha \frac{d\underline{\tau}(t)}{dt} \right)$ -space, each region  $\Lambda^{(k)}$  in the  $\Lambda$ -space corresponds to a region in the

$\left( \underline{\tau}(t) + \alpha \frac{d\underline{\tau}(t)}{dt} \right)$ -space.

Thus the solution is computed in the following way. Given that  $\underline{\tau}(t) + \alpha \frac{d\underline{\tau}(t)}{dt}$  belongs to the  $k$ -th

region of the  $\left( \underline{\tau}(t) + \alpha \frac{d\underline{\tau}(t)}{dt} \right)$ -space, then

$$\sum_{i \in m_k} R_{ij} u_i(t) = \sum_{i \in m_k} R_{ij} \left( \sum_{l=1}^D \lambda_l(t) R_{il} \right) = \sum_{l=1}^D \left( \sum_{i \in m_k} R_{ij} R_{il} \right) \lambda_l(t) = \tau_j(t) + \alpha \frac{d\tau_j(t)}{dt} \quad j = 1, 2, \dots, D, \text{ or}$$

$$\underline{\underline{R}}^{(k)T} \underline{\underline{R}}^{(k)} \underline{\lambda}(t) = \underline{\tau}(t) + \alpha \frac{d\underline{\tau}(t)}{dt},$$

where  $\underline{\underline{R}}^{(k)}$  is a matrix containing the rows of  $\underline{\underline{R}}$ , corresponding to the index group  $m_k$ . Hence,

$$\underline{\lambda}(t) = \left( \underline{\underline{R}}^{(k)T} \underline{\underline{R}}^{(k)} \right)^{-1} \left( \underline{\tau}(t) + \alpha \frac{d\underline{\tau}(t)}{dt} \right) \quad \text{and therefore}$$

$$(*) \quad \underline{U}(t) = \left[ \underline{\underline{R}} \left( \underline{\underline{R}}^{(k)T} \underline{\underline{R}}^{(k)} \right)^{-1} \left( \underline{\tau}(t) + \alpha \frac{d\underline{\tau}(t)}{dt} \right) \right]_+.$$

Equation (\*) provides the general solution to the optimization problem. This solution can be further simplified under the assumption of *generalized symmetry*, which is defined as independence of the expression  $\underline{\underline{R}}^{(k)T} \underline{\underline{R}}^{(k)}$  on the specific region  $k$ . Under this assumption, the expression  $\underline{\underline{R}}^{(k)T} \underline{\underline{R}}^{(k)}$  can be computed once, and there is no need to find the region to which  $\underline{\tau}(t) + \alpha \underline{\tau}'(t)$  belongs. In particular, the condition of generalized symmetry holds in the case of *strict symmetry*, implying that muscles are composed from symmetric antagonist pairs. Namely, for each pair of antagonist muscles  $i$  and  $i'$ ,  $R_{i',j} = -R_{ij}$ ,  $j = 1, 2, \dots, D$ . For a given region  $k$ , either  $i \in m_k$ , or  $i' \in m_k$ , and since

$R_{ij}R_{il} = (-R_{ij})(-R_{il}) = R_{i'j}R_{i'l}$ ,  $j, l \in (1, 2, \dots, D)$ , the expression  $\sum_{i \in m_k} R_{ij}R_{il}$ , does not depend on the specific region  $k$ . Thus, under the assumption of strict symmetry, the expression  $\underline{\underline{R}}^{(k)T} \underline{\underline{R}}^{(k)}$  can be computed once, while the index group  $m_k$  can be any group that contains a single representative from each pair of antagonist muscles. The condition of generalized symmetry is less restrictive. For example, it suffices that  $\sum_{i \in group1} R_{ij}R_{il} = \sum_{i \in group2} R_{ij}R_{il}$  for two groups of flexors and extensors surrounding the same joint, while not requiring each of the muscles in the group to have a symmetric pair.

### Neural Activity

Having computed the MCSs,  $\{u_i(t)\}_{i=1}^M$ , we now ask how the neural activity of each control signal is divided between the neurons contributing to this control signal. Since the integrand of the cost function and the constraints depend only on  $n_{i,j}(t-d_{i,j})$ , the solution at a given time depends only on the integrand and the constraint at that time. Therefore, the optimal control problem can be replaced by the following optimization problem.

$$\min_{\{n_{i,j}(t-d_{i,j})\}_{j=1}^{N_i}} \sum_{j=1}^{N_i} f(w_{i,j}n_{i,j}(t-d_{i,j})), \quad t_0 \leq t \leq t_f, \quad i=1, 2, \dots, M$$

s.t. (i)  $\sum_{j=1}^{N_i} w_{i,j}n_{i,j}(t-d_{i,j}) - u_i(t) = 0$

(ii)  $n_{i,j}(t-d_{i,j}) \geq 0 \quad j=1, 2, \dots, N_i$ .

Assume initially that the inequality constraints are absent. Using Lagrange multipliers we get that

$$f'(w_{i,j}n_{i,j}(t-d_{i,j})) \cdot w_{i,j} - \lambda \cdot w_{i,j} = 0 \quad j=1, 2, \dots, N_i, \quad ,$$

$$w_{i,j} \cdot n_{i,j}(t-d_{i,j}) = (f')^{-1}(\lambda) = const \quad j=1, 2, \dots, N_i, \quad ,$$

where  $(f')^{-1}$  exists due to the strictly convexity of  $f$ .

$$w_{i,j} n_{i,j}(t - d_{i,j}) = \frac{u_i(t)}{N_i} \quad j = 1, 2, \dots, N_i \text{ (due to the equality constraints)}$$

$$n_{i,j}(t - d_{i,j}) = \frac{u_i(t)}{N_i w_{i,j}} \quad j = 1, 2, \dots, N_i.$$

Since this solution obeys the inequality constraints, it serves as a solution of the full problem (including the inequality constraints). Thus, the neural activity of a single neuron  $n_{i,j}(t - d_{i,j})$  is proportional to the total neural activity of the control signal  $u_i(t)$ .

### *Isometric Task*

Consider an isometric task, i.e. the subject retains a fixed end-point position in the face of an external force field. Assume that the force is applied at a certain direction  $\varphi$  on the horizontal plane, namely

$$\underline{F}^{(ex)}(t) = F(t) \begin{bmatrix} \cos(\varphi) \\ \sin(\varphi) \\ 0 \end{bmatrix} = F(t) \underline{D}(\varphi).$$

According to the relation between end-point force and joint moments, given by Equation (3), we get that

$$\underline{\tau} = \underline{J}^T(\underline{\theta}) F(t) \underline{D}(\varphi)$$

and therefore

$$\underline{U}(t) = \left[ \underline{R} \left( \underline{R}^{(k)T} \underline{R}^{(k)} \right)^{-1} \underline{J}^T(\underline{\theta}) \left( F(t) + \alpha \frac{F(t)}{dt} \right) \underline{D}(\varphi) \right]_+$$

$$\underline{U}(t) = \left[ \left( F(t) + \alpha \frac{F(t)}{dt} \right) \underline{C}^{(k)}(\underline{\theta}) \underline{D}(\varphi) \right]_+$$

where  $\underline{C}^{(k)}(\underline{\theta}) = \underline{R} \left( \underline{R}^{(k)T} \underline{R}^{(k)} \right)^{-1} \underline{J}^T(\underline{\theta})$  is a  $M \times 3$  matrix.

Under the assumption of generalized symmetry mentioned above

$$\underline{C}^{(k)}(\underline{\theta}) = \underline{C}(\underline{\theta}) \quad \forall k$$

Hence

$$\underline{U}(t) = \left[ \left( F(t) + \alpha \frac{F(t)}{dt} \right) \underline{C}(\underline{\theta}) \underline{D}(\varphi) \right]_+ \text{ or}$$

$$u_i(t) = \left[ \left( F(t) + \alpha F'(t) \right) \left( C_{i,1}(\underline{\theta}) \cos(\varphi) + C_{i,2}(\underline{\theta}) \sin(\varphi) \right) \right]_+, \quad i = 1, 2, \dots, M$$

Using trigonometry we get that the tuning function is

$$u_i(t) = \left[ \left( F(t) + \alpha F'(t) \right) r_i(\underline{\theta}) \cos(\varphi - \varphi_i(\underline{\theta})) \right]_+, \quad i = 1, 2, \dots, M,$$

$$\text{where } r_i(\underline{\theta}) = \sqrt{C_{i,1}^2 + C_{i,2}^2} \quad \varphi_i(\underline{\theta}) = \text{tg}^{-1} \left( \frac{C_{i,2}}{C_{i,1}} \right) \quad i = 1, 2, \dots, M.$$

*Influence of gravity*

In the case where the arm is subject to gravity, some constant term is added to each torque, according to Equation (4). Therefore

$$u_i(t) = \left[ rg_i(\underline{\theta}) + \left( F(t) + \alpha F'(t) \right) r_i(\underline{\theta}) \cos(\varphi - \varphi_i(\underline{\theta})) \right]_+ \quad i = 1, 2, \dots, M,$$

where  $rg_i(\underline{\theta})$  is a constant bias due to gravity.

As before, the tuning function is a truncated cosine. However, the width of the tuning function is not exactly  $180^\circ$ , but wider or narrower, depending on the sign of the constant bias  $rg_i(\underline{\theta})$ .

## Appendix B

*Solution for the Bi-joint 6-Muscles Model*

The kinematic equations of a bi-joint planar arm (see Fig. 2a) are given by

$$\begin{aligned} x &= L_1 \cos(\theta_1) + L_2 \cos(\theta_1 + \theta_2) \\ y &= L_1 \sin(\theta_1) + L_2 \sin(\theta_1 + \theta_2) \quad , \end{aligned}$$

where  $L_1, L_2, \theta_1, \theta_2$  are explained in Fig. 2a.

The joint angles can be derived in this case solely from the hand position relative to the shoulder position, according to

$$\begin{aligned} \theta_1 &= \cos^{-1} \left( \frac{x}{\sqrt{x^2 + y^2}} \right) - \sin^{-1} \left( \frac{L_2 \sin(\theta_2)}{\sqrt{x^2 + y^2}} \right) \\ \theta_2 &= \cos^{-1} \left( \frac{x^2 + y^2 - L_1^2 - L_2^2}{2L_1 L_2} \right) \end{aligned}$$

Using these equations we have calculated joint angle trajectories. For the isometric task it was assumed that the hand position is (-5cm, 20cm) in shoulder coordinates. For the movement task it was assumed that the hand trajectory is a minimum jerk trajectory (Flash & Hogan, 1985), i.e.

$$\begin{aligned} x(t) &= x_0 + (x_0 - x_f)(15r^4 - 6r^5 - 10r^3) \\ y(t) &= y_0 + (y_0 - y_f)(15r^4 - 6r^5 - 10r^3) \quad , \end{aligned}$$

where  $r = \frac{t}{t_f}$ ;  $x_0, y_0$  and  $x_f, y_f$  are hand coordinates at  $t=0$  and at  $t = t_f$  respectively.

The static torque was calculated according to Equation (3), where the Jacobian in this case is given by

$$J = \begin{bmatrix} -L_1 \sin(\theta_1) - L_2 \sin(\theta_1 + \theta_2) & -L_2 \sin(\theta_1 + \theta_2) \\ L_1 \cos(\theta_1) + L_2 \cos(\theta_1 + \theta_2) & L_2 \cos(\theta_1 + \theta_2) \end{bmatrix} .$$

The dynamic torque was calculated according to Equation (4), which is given in explicit form for a bi-joint arm without gravity (see Fig. 2a) by

$$\begin{aligned} \tau_1 &= H_{11} \ddot{\theta}_1 + H_{12} \ddot{\theta}_2 - h\dot{\theta}_2^2 - 2h\dot{\theta}_1 \dot{\theta}_2 \\ \tau_2 &= H_{22} \ddot{\theta}_2 + H_{12} \ddot{\theta}_1 + h\dot{\theta}_1^2 \quad , \end{aligned}$$

where

$$H_{11} = m_1 r_1^2 + I_1 + m_2 [L_1^2 + r_2^2 + 2L_1 r_2 \cos(\theta_2)] + I_2$$

$$H_{22} = m_2 r_2^2 + I_2$$

$$H_{12} = m_2 L_1 r_2 \cos(\theta_2) + m_2 r_2^2 + I_2$$

$$h = m_2 L_1 r_2 \sin(\theta_2) \quad ,$$

$m_i$  is the mass of link  $i$ ,  $r_i$  is the distance between the joint and the center of link  $i$  and  $I_i$  is the inertia of link  $i$ . We used the following parameter values, applicable to a Rhesus monkey, based on Cheng and Scott (2000), Melis et al. (2002) and Graham and Scott (2003).

$$\begin{aligned} M_1 &= 0.29kg & M_2 &= 0.25kg \\ L_1 &= 14.4cm & L_2 &= 15.4cm \\ I_1 &= 2.2 \cdot 10^{-4} kg \cdot m^2 & I_2 &= 6.7 \cdot 10^{-4} kg \cdot m^2 \quad . \end{aligned}$$

Given the static and the dynamic torque, we have calculated the total torque according to equation (2).

The musculoskeletal geometry is given by six equivalent muscles, corresponding to the six classes of anatomical arm muscles: shoulder flexor and extensor, bi-joint flexor and extensor, and elbow flexor and extensor (Fig. 2b). For this model we've used the moment arm values shown in Table 2. These values are rough averages of the moment arms reported in Graham and Scott (2003).

The arm moments matrix, under the symmetry conditions discussed in Appendix A, is given by

$$R = \begin{bmatrix} R_{1,1} & 0 \\ -R_{1,1} & 0 \\ R_{3,1} & R_{3,2} \\ -R_{3,1} & -R_{3,2} \\ 0 & R_{5,2} \\ 0 & -R_{5,2} \end{bmatrix} \quad \text{and therefore} \quad R^{(k)} = \begin{bmatrix} R_{1,1} & 0 \\ R_{3,1} & R_{3,2} \\ 0 & R_{5,2} \end{bmatrix} .$$

Then, the MCSs were computed according to Equation (11).

**Acknowledgements:**

We are grateful to Shy Shoham for his very helpful comments on the Manuscript, and to Lauren Sergio and John Kalaska for providing us with details about their experimental setup. The helpful and instructive comments by the anonymous reviewers are also gratefully acknowledged. This work was partially supported by the Ollendorff foundation at the Electrical Engineering department at the Technion and by grant number 2007-8 to Dr. Karniel from the National Institute for Psychobiology in Israel.

## References

- Ajemian R, Bullock D, Grossberg S.** Kinematic Coordinates In Which Motor Cortical Cells Encode Movement Direction. *Journal of Neurophysiology* 84: 2191-2203, 2000.
- Alexander GE, Crutcher MD.** Preparation for Movement: Neural Representations of Intended Direction in Three Motor Areas of the Monkey. *Journal of Neurophysiology* 64: 133-150, 1990.
- Amirikian B, Georgopoulos AP.** Directional tuning profiles of motor cortical cells. *Neuroscience Research*, 36(1):73-79, 2000.
- Asada H, Slotine JJE.** *Robot Analysis and Control*. New York: Wiley Interscience, 2000.
- Ashe J.** What Is Coded in the Primary Motor Cortex? In: *Motor Cortex in Voluntary Movements*, edited by Riehle A, Vaadia E, London: CRC Press, 2005, p. 141-156.
- Baraduc P, Guigon E, Burnod Y.** Recoding Arm Position to Learn Visuomotor Transformations. *Cerebral Cortex* 11:906-917, 2001.
- Bernstein N.** *The Co-ordination and Regulation of MOVEMENTS*. London: Pergamon Press, 1967.
- Bizzi E, Mussa-Ivaldi FA, Giszter SF.** Computations underlying the execution of movement: a biological perspective. *Science* 253:287-291, 1991.
- Bolhuis BM & Gielen CCAM.** A comparison of models explaining muscle activation patterns for isometric contractions. *Biol. Cybern.* 81:249-261, 1999.
- Burke RE.** Spinal Cord: Ventral Horn. In: *The Synaptic Organization of the Brain Fifth Edition*, edited by Shepherd GM. New York: Oxford University Press, 2004, p. 79–123.
- Bryson AE.** *Dynamic Optimization*. Melno Park, California: Assison-Wesley, 1999.
- Bullock D, Grossberg S.** Neural Dynamics of Planned Arm Movements: Emergent Invariants and Speed-Accuracy Properties During Trajectory Formation. *Psychological Review* 95(1): 49-90, 1988.
- Burdet E, Milner TE.** Quantization of human motions and learning of accurate movements. *Biol. Cybern.* 78:307-318, 1998.
- Caminiti R, Johnson PB, Galli C, Ferraina S, Burnod Y.** Making arm movements within different parts of space: the premotor and motor cortical representations of a coordinate system for reaching to visual targets *The Journal of Neuroscience* 11: 1182-1197, 1991.

- Cheng EJ, Scott SH.** Morphometry of macaca mulatta forelimb. I shoulder and elbow muscles and segment inertial parameters. *J. Morphology*. 245: 206–224, 2000.
- Chow CK, Jacobson DH.** Studies of Human Locomotion Via Optimal Programming. *Math. Biosci.* 10:239-306, 1971.
- Cisek P, Grossberg S, Bullock D.** A Cortico-Spinal Model of Reaching and Proprioception under Multiple Task Conditions. *Journal of Cognitive Neuroscience* 10(4): 425–444, 1998.
- Crutcher MD, Alexander GE.** Movement-Related Neuronal Activity Selectively Coding Either Direction or Muscle Pattern in Three Motor Areas of the Monkey. *Journal of Neurophysiology* 64: 151-163, 1990.
- Dum RP, Strick PL.** Motor areas in the frontal lobe: the anatomical substrate for the central control of movement. In: *Motor Cortex in Voluntary Movements*, edited by Riehle A, Vaadia E. London: CRC Press, 2005, p. 3-47.
- Engelbrecht S.** Minimum principles in motor control. *J. Math. Psychol.* 45(3): 497–542, 2001.
- Evarts EV.** Relation of Pyramidal Tract Activity to Force Exerted During Voluntary Movement. *Journal of Neurophysiology* 31(1): 14-27, 1968.
- Fetz EE, Cheney PD.** Postspike Facilitation of Forelimb Muscle Activity by Primate Corticomotoneuronal cells. *Journal of Neurophysiology* 44: 751–772, 1980.
- Flash T, Hogan N.** The Coordination of Arm Movements: An Experimentally Confirmed Mathematical Model. *The Journal of Neuroscience* 5(7): 1688-1703, 1985.
- Carpenter GA, Cohen MA, Grossberg S, Kohonen T, Oja E, Palm G, Hopfield JJ.** Computing with Neural Networks. *Science* 235(4793): 1226-1228, 1987.
- Garner BA, Pandy MG.** Musculoskeletal model of the human arm based on the Visible Human Male dataset. *Computer Methods in Biomechanics and Biomedical Engineering* 4: 93-126, 2001.
- Georgopoulos AP, Kalaska JF, Caminiti R, Massey JT.** On the relation between the direction of two-dimensional arm movements and cell discharge in primate motor cortex. *The Journal of Neuroscience* 11: 1527–1537, 1982.
- Georgopoulos AP, Kalaska JF, Massey J.** Spatial coding of movements: A hypothesis concerning the coding of movement direction by motor cortical populations. *Experimental Brain Research (Supp.)* 7: 327–336, 1983.

- Graham KM, Scott SH.** Morphometry of macaca mulatta forelimb. III moment arm of shoulder and elbow muscles. *J. Morphology*. 255: 301–314, 2003.
- Harris CM, Wolpert DM.** Signal-dependent noise determines motor planning. *Nature* 394: 780-784, 1998.
- Hocherman S, Wise SP.** Effects of hand movement path on motor cortical activity in awake, behaving rhesus monkeys. *Exp Brain Res* 83: 285-302, 1991.
- Hogan N.** Adaptive Control of Mechanical Impedance by Coactivation of Antagonist Muscles. *IEEE Transactions on Automatic control AC* 29(8): 681-690, 1984.
- Hogan N.** Mechanical Impedance of Single and Multi-Articular Systems. In: *Multiple Muscle Systems Biomechanics and Movement Organization*, edited by Winters JM, Woo SLY. New York: Springer-Verlag, 1989, p 149–164.
- Humphrey DR.** Relating Motor Cortex Spike Trains to Measure of Motor Performance. *Brain Research* 40:7-12, 1972.
- Johnson M, Mason C, Ebner T.** Central processes for the multiparametric control of arm movements in primates. *Current Opinion in Neurobiology* 2(11): 684–688, 2001.
- Kakei S, Hoffman DS, Strick PL.** Muscle and movement representations in the primary motor cortex. *Science* 285(5436): 2136–2139, 1999.
- Kandel ER, Schwartz JH, Jessel TM.** *Principles of Neural Science*. New York: McGraw-Hill, fourth edition, 2001.
- Lacquaniti F, Guigon E, Bianchi L, Ferraina S, Caminiti R.** Representing spatial information for limb movement: role of area 5 in the monkey. *Cerebral Cortex* 5:391-409, 1995.
- Loeb GE, Brown IE, Lan N, Davoodi R.** The importance of biomechanics. *Adv. Exp. Med. Biol.* 508: 481-487, 2002.
- Melis EH, Richmond FJR, Singh K, Scott SH.** Morphometry of macaca mulatta forelimb. II fiber-type composition in shoulder and elbow muscles. *J. Morphology*. 251: 323– 332, 2002.
- Miyamoto H, Nakano E, Wolpert DM, Kawato M.** TOPS (Task Optimization in the Presence of Signal-Dependent Noise) Model. *Systems and Computers in Japan* 35(11): 48-58, 2004.
- Moran DW, Schwartz AB.** Letters to the editor. *Nature Neuroscience* 3(10): 963, 2000.

- Morasso P.** Spatial Control of Arm Movements. *Exp Brain Res* 42:223-227, 1981.
- Morrow MM, Miller LE.** Prediction of muscle activity by populations of sequentially recorded primary motor cortex neurons. *Journal of Neurophysiology* 89(4): 2279–2288, 2003.
- Mussa-Ivaldi FA.** Do neurons in the motor cortex encode movement direction? an alternative hypothesis. *Neuroscience Letters* 91: 106–111, 1988.
- Neilson PD, Neilson MD.** Motor Maps and Synergies. *Human Movement Science* 24: 774-797, 2005.
- Osu R, Kamimura N, Iwasaki H, Nakano E, Harris CM, Wada Y, Kawato M.** Optimal Impedance Control for Task Achievement in the Presence of Signal-Dependent Noise. *Journal of Neurophysiology* 92: 1199-1215, 2004.
- Pandy MG.** Computer modeling and simulation of human movement. *Annu. Rev. Biomed. Eng.* 3: 245–273, 2001.
- Paninski L, Shoham S, Fellows MR, Hatsopoulos NG and Donoghue JP.** Superlinear Population Encoding of Dynamic Hand Trajectory in Primary Motor Cortex. *The Journal of Neuroscience*, 24(39):8551– 8561, 2004.
- Salinas E, Abbott LF.** Vector reconstruction from firing rates. *J. Comput. Neurosci.* 1: 89-107, 1994.
- Sanger TD.** Theoretical Considerations for the Analysis of Population Coding in Motor Cortex. *Neural Computation* 6: 29-37, 1994.
- Sanger TD.** Probability Density Estimation for the Interpretation of Neural Population Codes. *Journal of Neurophysiology* 76(4): 2790-2793, 1996.
- Schwartz, AB.** Cortical neural prosthetics. *Annual Review of Neuroscience*, 27, 487-507, 2004.
- Scott SH, Gribble PL, Graham KM, Cabel DW.** Dissociation between hand motion and population vectors from neural activity in motor cortex. *Nature* 417: 938-941, 2002.
- Scott SH, Kalaska JF.** Reaching Movements with Similar Hand Paths but Different Arm Orientations. I. Activity of Individual Cells in Motor Cortex. *Journal of Neurophysiology* 77: 826–852, 1997.
- Sergio LE, Hamel-Pêquet C, Kalaska JF.** Motor cortex neural correlates of output kinematics and kinetics during isometric-force and arm-reaching tasks. *Journal of Neurophysiology* 94: 2353-2378, 2005.

**Sergio LE, Kalaska JF.** Systematic changes in directional tuning of motor cortex cell activity with hand location in the workspace during generation of static isometric forces in constant spatial directions. *Journal of Neurophysiology* 78: 1170–1174, 1997.

**Sergio LE, Kalaska JF.** Changes in the temporal pattern of primary motor cortex activity in a directional isometric force versus limb movement task. *Journal of Neurophysiology* 80: 577–1583, 1998.

**Sergio LE, Kalaska JF.** Systematic Changes in Motor Cortex Cell Activity With Arm Posture During Directional Isometric Force Generation. *Journal of Neurophysiology* 89: 212–228, 2003.

**Shadmehr R, Mussa-Ivaldi FA.** Adaptive Representation of Dynamics during Learning of a Motor Task. *The Journal of Neuroscience* 14(5): 3208-3244, 1994.

**Shpigelman L, Singer Y, Paz R, Vaadia E.** Spikernels: Predicting Arm Movements by Embedding Population Spike Rate Patterns in Inner-Product Spaces. *Neural. Computation.* 17: 671–690, 2005.

**Spong MW, Hutchinson S, Vidyasagar M.** *Robot Modeling and Control.* John Wiley and Sons, 2006.

**Taylor DM, Helms Tillery SI, Schwartz AB.** Direct cortical control of 3D neuroprosthetic devices. *Science* 296:1829–32, 2002.

**Thach WT.** Correlation of Neural Discharge with Pattern and Force of Muscular Activity, Joint Position, and Direction of Intended Next Movement in Motor Cortex and Cerebellum. *Journal of Neurophysiology* 41: 654–676, 1978.

**Todorov E.** Direct cortical control of muscle activation in voluntary arm movements: a model. *Nature Neuroscience* 3: 391–398, 2000.

**Todorov E.** On the role of primary motor cortex in arm movement control. *In Progress in Motor Control,* III 6: 125–166, 2002.

**Torres E, Andersen R.** Space-Time Separation During Obstacle-Avoidance Learning in Monkeys. *Journal of Neurophysiology* 96:2613-2632, 2006.

**Wu W, Black MJ, Gau Y, Bienenstock E, Donoghue JP.** Modeling and Decoding Motor Cortical Activity Using a Switching Kalman Filter. *IEEE Transactions on Biomedical Engineering* 51(6): 933-942, 2004.

## Figure Legends

Figure 1: Overview.

a: General model block diagram. b: Solution flow chart and the general model's parameters.

Figure 2: Arm model with 2 joints and 6 muscles.

a: Arm Mechanics.  $L_1$  and  $L_2$  are the upper arm and forearm lengths respectively.  $\theta_1$  and  $\theta_2$  are the shoulder and elbow angles respectively.  $\tau_1$  and  $\tau_2$  are the shoulder and elbow torques respectively.  $\underline{P} = (x, y)$  are hand coordinates relative to the shoulder at  $(0, 0)$ .  $\underline{F}$  is the force vector exerted by the hand. b:

Equivalent Muscles. Sh = Shoulder, Bi = Bi-joint, El = Elbow, F = Flexor, E = Extensor.

Figure 3: Directional tuning of the muscle control signals.

a: Tuning functions for the 2-DOF-arm model. Right hand position is  $(-5\text{cm}, 20\text{cm})$ . Sh = Shoulder, Bi = Bi-joint, El = Elbow, F = Flexor, E = Extensor. b: Preferred directions for the 2-DOF-arm model.

Parameters and notations are the same. c: PD at different locations of the right hand for a neuron related to the bi-joint flexor according to the 2-DOF-arm model (Appendix B). The position of each arrow corresponds to the relative location of the hand on the planar work surface, with the top arrow corresponding to the most distal hand location. The central location is  $(-5\text{cm}, 20\text{cm})$ . The remaining 8 hand locations were at a distance of 8cm, spaced at  $45^\circ$  intervals, starting at  $0^\circ$ . The arrow represents the PD with respect to the isometric force. d: Cell directional response in the isometric task, based on Fig. 1a from Sergio and Kalaska (1998), with permission. Discharge pattern of a shoulder-related M1 cell during the isometric force task. Each raster illustrates cell activity during 5 trials, and the raster location corresponds to the direction of the force. Data are aligned on the 1st significant force change, denoted by a solid vertical line (M). For each trial, the heavy tick mark to the left of the cursor movement onset line shows the time of target onset and the heavy tick mark to the right shows the time at which the final static level of force within the peripheral target was attained. It can be seen that after the force change (M) the response is about zero in four out of eight directions. Therefore, the tuning function width is about  $180^\circ$ .

Figure 4: Pulse step response in the isometric task for the general model.

The ordinate is normalized to arbitrary units. a: Step of muscle force. b: First derivative of muscle force. c: Combined pulse step response. Solid bold line:  $\alpha = 100\text{ms}$ . Solid line:  $\alpha = 200\text{ms}$ . Dotted line:  $\alpha = 300\text{ms}$ .

Figure 5: Population activity for the isometric task for the general model.

a: Experiment, based on Fig. 9 of Sergio et al. (2005), with permission. Mean population response as a function of time and force direction, where the direction is relative to the PD of each cell. All data were aligned to the time of force onset (time 0) and the PD of each neuron was arbitrarily rotated to the right. b: Simulation of the average neural response in our model. The ordinate of the simulation is normalized to arbitrary units.

Figure 6: Isometric task – single cell response for the general model.

a: Experiment, based on Fig. 1a from Sergio and Kalaska (1998), with permission. Discharge pattern at the PD (upper) and at the opposite direction (lower) of a shoulder-related M1 cell in histogram format (10-ms bins). Data are aligned on the first significant force change, denoted by a solid vertical line (M). b: Simulation of our model at the PD (upper) and at the opposite direction (lower). We assumed that the control signal is delayed by 100ms. The ordinate of the simulation is normalized to the same arbitrary units as in Fig. 5b.

Figure 7: Tri-phasic response in the movement task for the general model.

a: Hand inertial force during a minimum jerk trajectory, given by  $F(r) \propto 2r^3 - 3r^2 + r$ , where  $r = t/t_f$  (the units are arbitrary). b:  $F(t) + \alpha F'(t)$ . The positive phases (the first and the third) represent the profile of one MCS. The negative phase (the second) represents the profile of the antagonist MCS. c: Shoulder muscle torques in the 2-DOF-arm model for the movement task. Movement direction is 0. The dashed line is the shoulder flexor torque, the dotted line is the shoulder extensor torque, and the solid line is the total torque. Vertical lines denote transitions between antagonist control signals. d: The influence of the value of  $\alpha$  (force derivative coefficient) on cell response at the PD. Solid bold line:  $\alpha = 100\text{ms}$ . Solid line:  $\alpha = 200\text{ms}$ . Dotted line:  $\alpha = 300\text{ms}$ . e: The same as d at the opposite direction.

Figure 8: Population activity in the movement task for the general model.

a: Experiment, based on Fig. 9 of Sergio et al. (2005), with permission. Mean population response as a function of time and force direction, where the direction is relative to the PD of each cell. All data were aligned to the time of force onset (time 0) and the PD of each neuron, calculated at target hold time, was arbitrarily rotated to the right. b: Simulation of a MCS in our model. The ordinate of the simulation of our control signal is normalized to the same arbitrary units as in Fig. 5b.

Figure 9: Movement task – single cell response for the general model.

a: Experiment, based on Fig. 1b from Sergio and Kalaska (1998), with permission. Discharge pattern at the PD (upper) and at the opposite direction (lower) of a shoulder-related M1 cell in histogram format (10-ms bins). Data are aligned on the first significant force change, denoted by a solid vertical line (M). b: Simulation of the single neuron activity at the PD (upper) and at the opposite direction (lower). We assume a delay of 100ms. The ordinate of simulation is normalized to the same arbitrary units as in Fig. 5b. c: Reconstruction of Fig. 2C in Todorov (2002). Activity at the PD (upper) and at the opposite direction (lower).

Figure 10: Reversals of the PD during movement task.

a: Based on Fig. 2b of Sergio and Kalaska (1998), with permission. The temporal trajectory of the PD of a representative cell during movement tasks. The trajectory was determined by a 50ms sliding-window analysis. Time windows within which the cell was significantly related to direction are shown by an asterisk. Time windows within which the cell was not directionally related are shown by circle. Notice that around the transition times (characterized by reversal of PD) the cell was not directionally tuned. Large thick concentric circles denote movement onset and offset. b: Simulation of a single neuron PD in the 2-DOF-arm model. The PD was calculated as the angle at which the tuning function attains its maximum. The PD is relative to its value during target hold time. c: The temporal tuning function in the 2-DOF-arm model for the movement task at time = 80 ms.

**Tables**

<b>Variables</b>	<b>Notation</b>	<b>Figure</b>	<b>Equations</b>
End point position	$\underline{P} = (P_1, \dots, P_N)$	2a	1
End point force	$\underline{F}^{(ex)} = (F_1^{(ex)}, \dots, F_N^{(ex)})$	2a	2
Joint angles	$\underline{\theta} = (\theta_1, \theta_2, \dots, \theta_D)^T$	2a	1,3,4
Joint torques	$\underline{\tau} = (\tau_1, \tau_2, \dots, \tau_D)^T$	2a	2,3,4,5
Muscle forces	$\underline{F} = (F_1, F_2, \dots, F_M)^T$	2b	5,6
MCSs	$\underline{U} = (U_1, U_2, \dots, U_M)^T$	2b	6,7,8
Single neuron activities	$n_{i,j} \quad j = 1, 2, \dots, N_i \quad i = 1, 2, \dots, M$		7,9

Table 1: Model variables.

<b>Equivalent Muscle</b>	<b>Shoulder Moment Arm</b>	<b>Elbow Moment Arm</b>
Shoulder flexor	$R_{1,1} = 2cm$	$R_{1,2} = 0$
Shoulder extensor	$R_{2,1} = -R_{1,1} = -2cm$	$R_{2,2} = 0$
Bi-joint flexor	$R_{3,1} = 2cm$	$R_{3,2} = 1.5cm$
Bi-joint extensor	$R_{4,1} = -R_{3,1} = -2cm$	$R_{4,2} = -R_{3,2} = -1.5cm$
Elbow flexor	$R_{5,1} = 0$	$R_{5,2} = 2cm$
Elbow extensor	$R_{6,1} = 0$	$R_{6,2} = -R_{5,2} = -2cm$

Table 2: Moment arms of the 2-DOF-arm model.

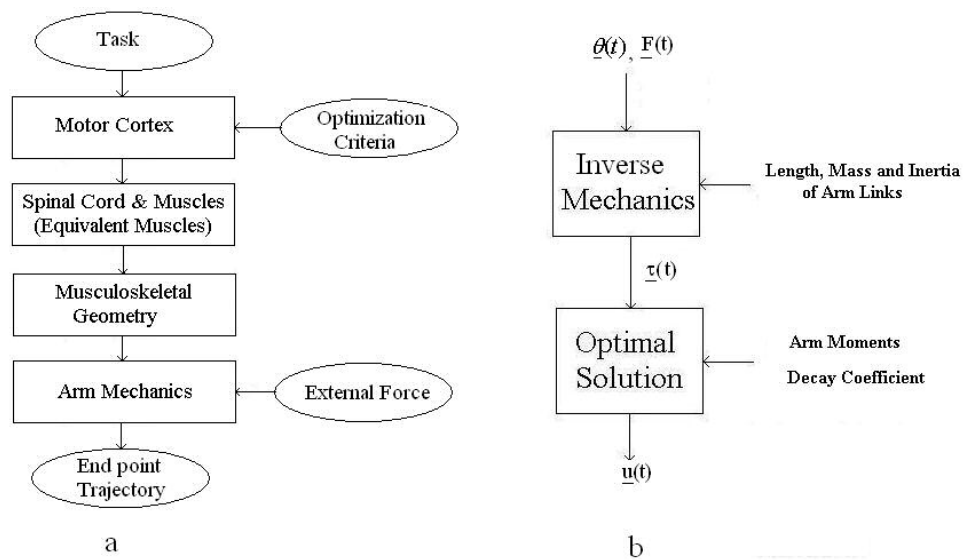


**Figure 1: Overview. a: General model block diagram. b: Solution flow chart and the general model's parameters.**

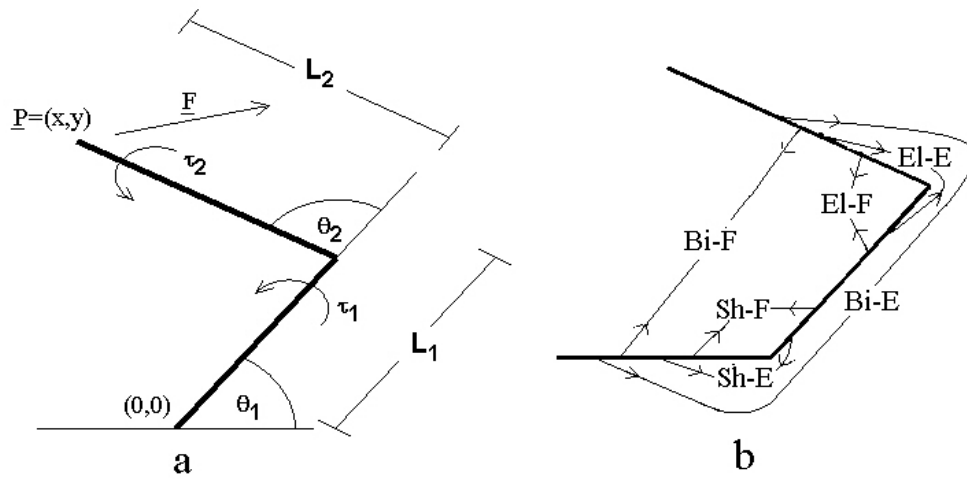


**Figure 2: Arm model with 2 joints and 6 muscles. a: Arm Mechanics.  $L_1$  and  $L_2$  are the upper arm and forearm lengths respectively.  $\theta_1$  and  $\theta_2$  are the shoulder and elbow angles respectively.  $\tau_1$  and  $\tau_2$  are the shoulder and elbow torques respectively.  $\underline{P}=(x,y)$  is the hand coordinates relative to the shoulder at  $(0,0)$ .  $\underline{F}$  is the force vector exerted by the hand. b: Equivalent Muscles. Sh = Shoulder, Bi = Bi-joint, El = Elbow, F = Flexor, E = Extensor.**

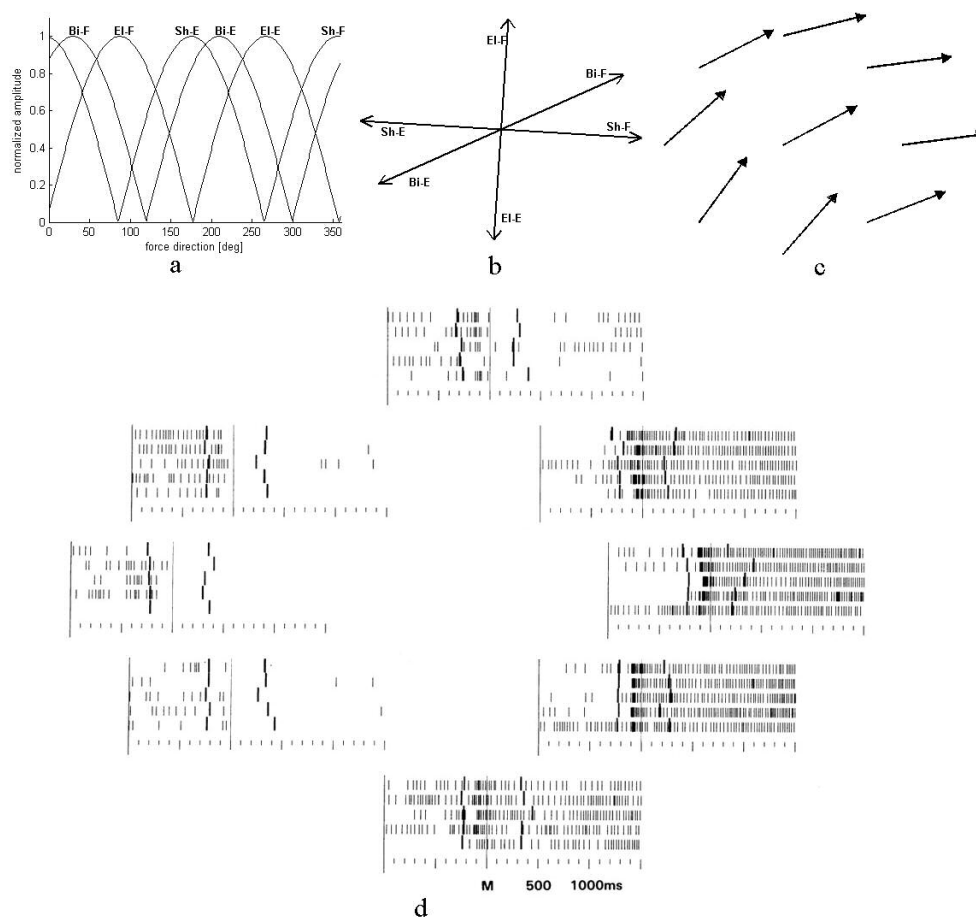


**Figure 3: Directional tuning of the muscle control signals. a: Tuning functions for the 2-DOF-arm model. Right hand position is ( 5cm, 20cm). Sh = Shoulder, Bi = Bi-joint, El = Elbow, F = Flexor, E = Extensor. b: Preferred directions for the 2-DOF-arm model. Parameters and notations are the same. c: PD at different locations of the right hand for a neuron related to the bi-joint flexor according to the 2-DOF-arm model (Appendix B). The position of each arrow corresponds to the relative location of the hand on the planar work surface, with the top arrow corresponding to the most distal hand location. The central location is ( 5cm, 20cm). The remaining 8 hand locations were at a distance of 8cm, spaced at  $45^\circ$  intervals, starting at  $0^\circ$ . The arrow represents the PD with respect to the isometric force. d: Cell directional response in the isometric task, based on Fig. 1a from Sergio and Kalaska (1998), with permission. Discharge pattern of a shoulder-related M1 cell during the isometric force task. Each raster illustrates cell activity during 5 trials, and the raster location corresponds to the direction of the force. Data are aligned on the 1st significant force change, denoted by a solid vertical line (M). For each trial, the heavy tick mark to the left of the cursor movement onset line shows the time of target onset and the heavy tick mark to the right shows the time at which the final static level of force within the peripheral target was attained. It can be seen that after the force change (M) the response is about zero in four out of eight directions. Therefore, the tuning function width is about  $180^\circ$ .**

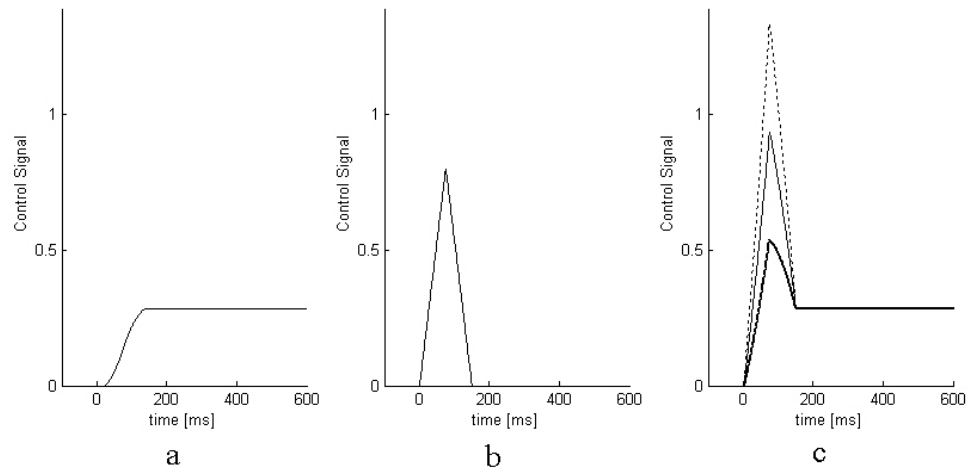


**Figure 4: Pulse step response in the isometric task for the general model. The ordinate is normalized to arbitrary units. a: Step of muscle force. b: First derivative of muscle force. c: Combined pulse step response. Solid bold line:  $\alpha = 100\text{ms}$ . Solid line:  $\alpha = 200\text{ms}$ . Dotted line:  $\alpha = 300\text{ms}$ .**

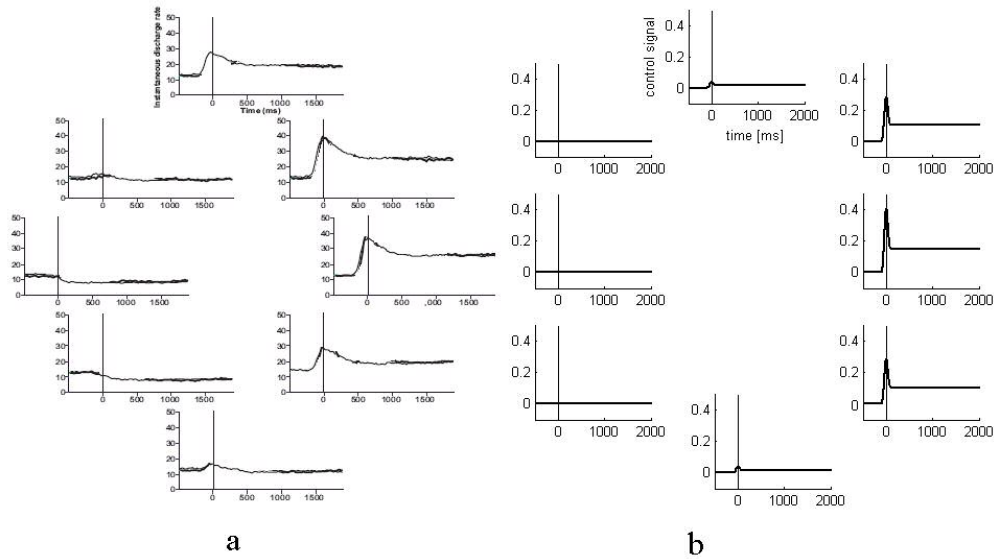


**Figure 5: Population activity for the isometric task for the general model. a: Experiment, based on Fig. 9 of Sergio et al. (2005), with permission. Mean population response as a function of time and force direction, where the direction is relative to the PD of each cell. All data were aligned to the time of force onset (time 0) and the PD of each neuron was arbitrarily rotated to the right. b: Simulation of the average neural response in our model. The ordinate of the simulation is normalized to arbitrary units.**

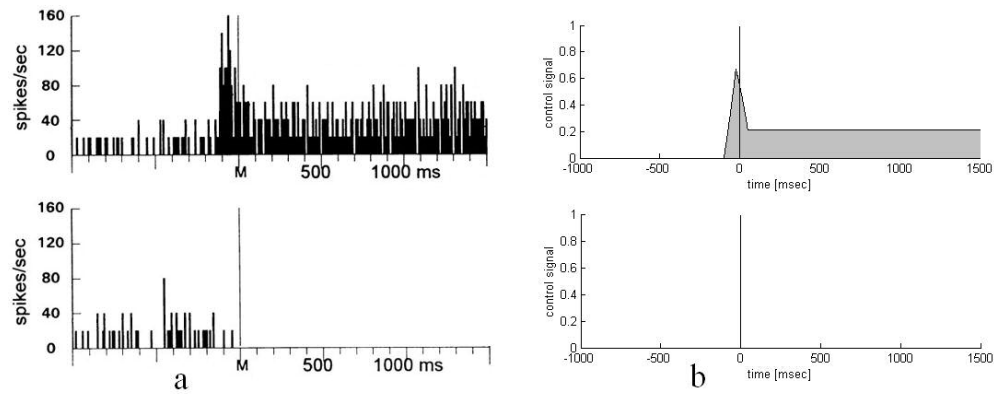


**Figure 6: Isometric task □ single cell response for the general model. a: Experiment, based on Fig. 1a from Sergio and Kalaska (1998), with permission. Discharge pattern at the PD (upper) and at the opposite direction (lower) of a shoulder-related M1 cell in histogram format (10-ms bins). Data are aligned on the first significant force change, denoted by a solid vertical line (M). b: Simulation of our model at the PD (upper) and at the opposite direction (lower) . We assumed that the control signal is delayed by 100ms. The ordinate of the simulation is normalized to the same arbitrary units as in Fig. 5b.**

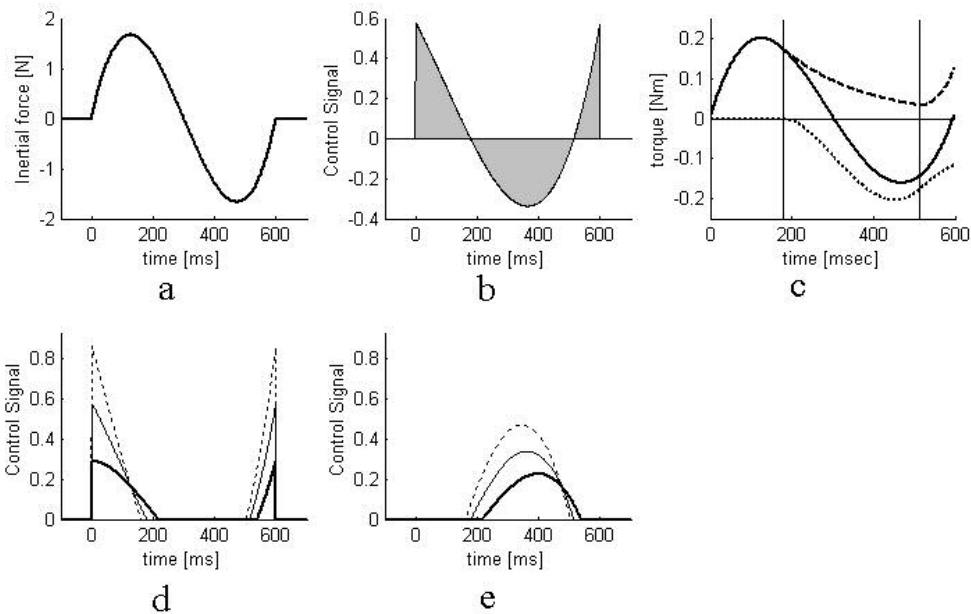


**Figure 7: Tri-phasic response in the movement task for the general model. a: Hand inertial force during a minimum jerk trajectory, given by  $F = m \cdot \ddot{x}$ , where  $m$  (the units are arbitrary). b:  $\tau$ . The positive phases (the first and the third) represent the profile of one MCS. The negative phase (the second) represents the profile of the antagonist MCS. c: Shoulder muscle torques in the 2-DOF-arm model for the movement task. Movement direction is 0. The dashed line is the shoulder flexor torque, the dotted line is the shoulder extensor torque, and the solid line is the total torque. Vertical lines denote transitions between antagonist control signals. d: The influence of the value of  $\alpha$  (force derivative coefficient) on cell response at the PD. Solid bold line:  $\alpha = 100\text{ms}$ . Solid line:  $\alpha = 200\text{ms}$ . Dotted line:  $\alpha = 300\text{ms}$ . e: The same as d at the opposite direction.**

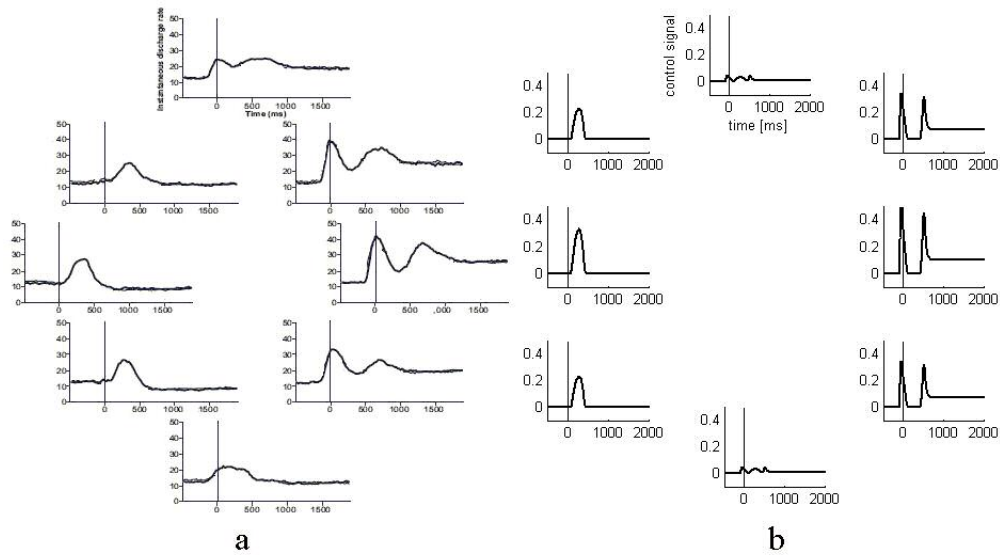


**Figure 8: Population activity in the movement task for the general model. a: Experiment, based on Fig. 9 of Sergio et al. (2005), with permission. Mean population response as a function of time and force direction, where the direction is relative to the PD of each cell. All data were aligned to the time of force onset (time 0) and the PD of each neuron, calculated at target hold time, was arbitrarily rotated to the right. b: Simulation of a MCS in our model. The ordinate of the simulation of our control signal is normalized to the same arbitrary units as in Fig. 5b.**

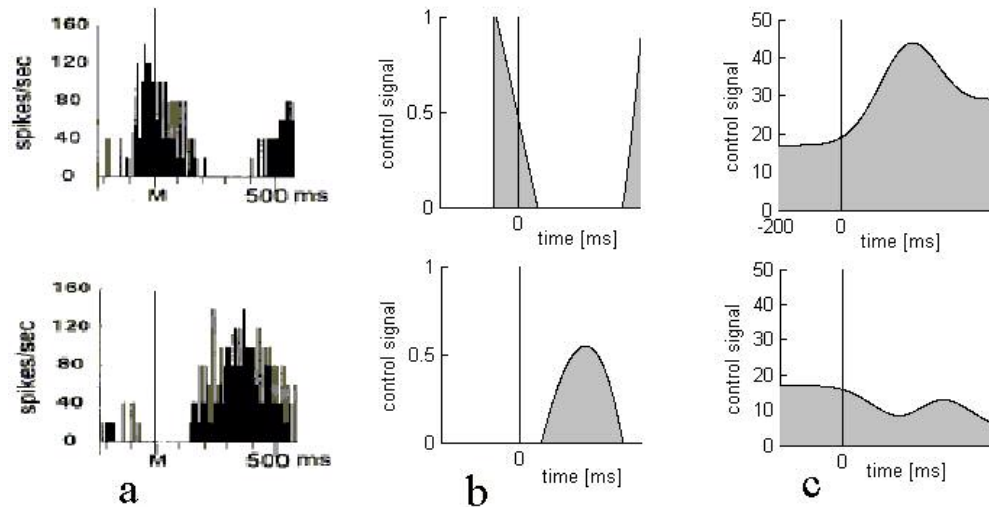


**Figure 9: Movement task  $\square$  single cell response for the general model. a: Experiment, based on Fig. 1b from Sergio and Kalaska (1998), with permission. Discharge pattern at the PD (upper) and at the opposite direction (lower) of a shoulder-related M1 cell in histogram format (10-ms bins). Data are aligned on the first significant force change, denoted by a solid vertical line (M). b: Simulation of the single neuron activity at the PD (upper) and at the opposite direction (lower). We assume a delay of 100ms. The ordinate of simulation is normalized to the same arbitrary units as in Fig. 5b. c: Reconstruction of Fig. 2C in Todorov (2002). Activity at the PD (upper) and at the opposite direction (lower).**

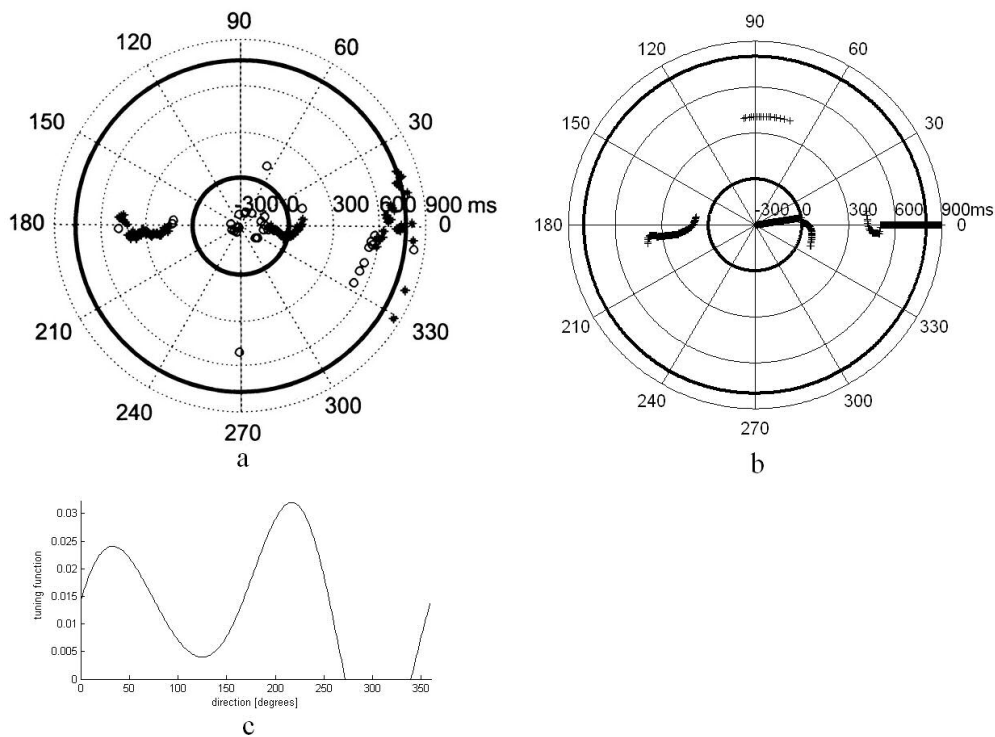


**Figure 10: Reversals of the PD during movement task. a: Based on Fig. 2b of Sergio and Kalaska (1998), with permission. The temporal trajectory of the PD of a representative cell during movement tasks. The trajectory was determined by a 50ms sliding-window analysis. Time windows within which the cell was significantly related to direction are shown by an asterisk. Time windows within which the cell was not directionally related are shown by circle. Notice that around the transition times (characterized by reversal of PD) the cell was not directionally tuned. Large thick concentric circles denote movement onset and offset. b: Simulation of a single neuron PD in the 2-DOF-arm model. The PD was calculated as the angle at which the tuning function attains its maximum. The PD is relative to its value during target hold time. c: The temporal tuning function in the 2-DOF-arm model for the movement task at time = 80 ms.**

Variables	Notation	Figure	Equations
End point position	$\underline{P} = (P_1, \dots, P_N)$	2a	1
End point force	$\underline{F}^{(ex)} = (F_1^{(ex)}, \dots, F_N^{(ex)})$	2a	2
Joint angles	$\underline{\theta} = (\theta_1, \theta_2, \dots, \theta_D)^T$	2a	1,3,4
Joint torques	$\underline{\tau} = (\tau_1, \tau_2, \dots, \tau_D)^T$	2a	2,3,4,5
Muscle forces	$\underline{F} = (F_1, F_2, \dots, F_M)^T$	2b	5,6
MCSs	$\underline{U} = (U_1, U_2, \dots, U_M)^T$	2b	6,7,8
Single neuron activities	$n_{i,j} \quad j = 1, 2, \dots, N_i \quad i = 1, 2, \dots, M$		7,9

Table 1: Model variables.

<b>Equivalent Muscle</b>	<b>Shoulder Moment Arm</b>	<b>Elbow Moment Arm</b>
Shoulder flexor	$R_{1,1} = 2cm$	$R_{1,2} = 0$
Shoulder extensor	$R_{2,1} = -R_{1,1} = -2cm$	$R_{2,2} = 0$
Bi-joint flexor	$R_{3,1} = 2cm$	$R_{3,2} = 1.5cm$
Bi-joint extensor	$R_{4,1} = -R_{3,1} = -2cm$	$R_{4,2} = -R_{3,2} = -1.5cm$
Elbow flexor	$R_{5,1} = 0$	$R_{5,2} = 2cm$
Elbow extensor	$R_{6,1} = 0$	$R_{6,2} = -R_{5,2} = -2cm$

Table 2: Moment arms of the 2-DOF-arm model.